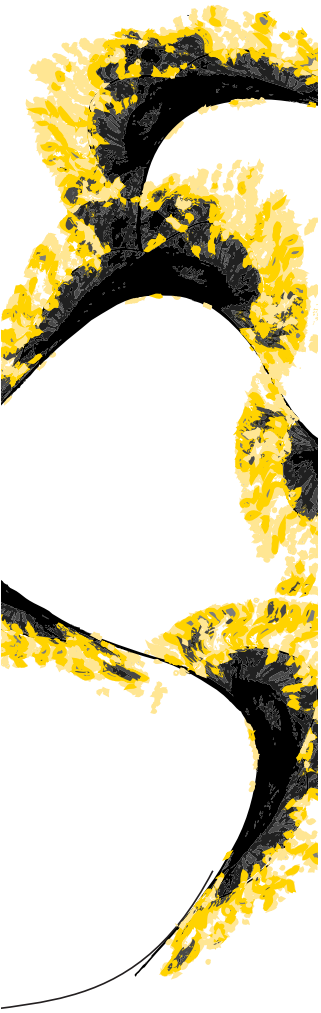

RAM ROBOTICS AND MECHATRONICS

DESIGN AND VALIDATION OF AN MRI COMPATIBLE ANTHROPOMORPHIC LIVER PHANTOM

J.S. (Joseph) Zacharias

MSC ASSIGNMENT

Committee:
dr. ir. M. Abayazid
V.R. Puranam, MSc
M.A.A. Atalla, MSc
dr. A. Sadeghi

December, 2024

080RaM2024
Robotics and Mechatronics
EEMCS
University of Twente
P.O. Box 217
7500 AE Enschede
The Netherlands

UNIVERSITY OF TWENTE. | TECHMED CENTRE UNIVERSITY OF TWENTE. | DIGITAL SOCIETY INSTITUTE

Abstract

Respiratory motion poses significant challenges in medical imaging procedures involving the liver, such as in biopsies and tumor ablations. The movement of organs caused by breathing can reduce the precision of needle insertions, increasing the risk of tissue trauma and other treatment complications. While existing liver phantoms can simulate respiratory motions, they often lack the realism of specific needle insertion boundaries and the robustness needed for accurate testing and validation, especially in Magnetic Resonance Imaging (MRI) compatible environments. In this thesis, an anthropomorphic liver phantom setup that replicates Superior-Inferior (SI) and Anterior-Posterior (AP) respiratory movements was developed and validated. The actuation of the phantom is done using MRI-compatible pneumatic origami actuators, chosen for their cost-effectiveness and force actuation capabilities. A soft rubber liver phantom housed within a 3D-printed ribcage was designed to mimic realistic anatomical constraints. The system operates with an open-loop Arduino control mechanism to recreate human breathing patterns, with the future potential to integrate closed loop control which will further enhance the accuracy and realism of the movements. The entire setup is modular and built from materials carefully selected for MRI compatibility. The results demonstrate that the phantom achieves controlled motion in both the SI and AP directions, validating its potential for simulating respiratory motion in a clinical context. The modularity of the design allows for easy maintenance and adaptability for further improvements. This work represents a step toward creating a more realistic and functional liver phantom, thereby contributing to safer and more effective liver procedures.

Contents

1 Introduction

Magnetic resonance imaging (MRI) plays a critical role in non-invasive medical procedures, particularly in procedures such as biopsies and tumor ablations. However, respiratory motion introduces significant challenges in ensuring the accuracy and safety of the patients during these procedures. Movement due to breathing can shift the position of the abdominal organs, thereby making it difficult for physicians to accurately locate and target tumors, which could lead to tissue trauma in the patient. To overcome these challenges, researchers have developed anthropomorphic phantoms that allow for simulation of respiratory motion, providing a safe environment for testing and refining medical interventions. These phantoms can offer physicians more practice in a more controlled environment without compromising on patient safety.

This chapter explains the main context of this thesis and briefly discusses its objective. It outlines the novelty and scope of the thesis and highlights potential limitations. Finally, it presents the remaining structure of the thesis.

1.1 Context

1.1.1 Respiratory motion

Respiratory motion presents significant challenges in the accurate targeting and treatment of thoracic and abdominal tumours. Some of these complications are that it takes more time and focus for the physician to accurately detect the location of a tumor and ablate it; another potential complication is the breathing movement causes the physician to miss critical needle insertion points, therefore requiring re-insertion of the needle, causing unwanted tissue trauma [1].
To address the aforementioned challenges, researchers have designed and developed respiratory motion robotic phantoms that mimic breathing motion of internal organs in humans. Realistic phantoms of thoracic and abdominal organs such as the liver are set atop these motion platforms and are used to test needle insertion procedures, instead of live humans being tested on.

1.1.2 Imaging and actuation

Magnetic Resonance Imaging (MRI) and Computed Tomography scans (CT scans) are common methods of medical imaging used to obtain detailed images of internal organs. These methods are commonly used to visualize internal structures without the need for invasive procedures, thereby minimising patient discomfort and risk of infection. Both imaging modalities have their advantages and disadvantages. CT scans are quicker and are better at spatial resolution albeit using ionising radiation and having a lower temporal resolution than MRI. MRI does not use radiation for imaging and can help cancer tissue stand out from regular tissue albeit that MRI scans take a lot longer than CT and anyone with a metal implant cannot partake in an MRI due to the strong magnetic field [2]. The test setups that are used inside the MRI bores should be made up of non-ferromagnetic materials because such materials can distort produced images with artefacts [3]. A common method to control moving components inside MRI machines are soft pneumatic actuators. This is because these actuators are light, inexpensive to manufacture, and above all they do not use materials that result in image artefacts of the scans; this makes them a valuable tool for this particular field of biomedical research [4].

1.1.3 Control algorithms for breathing

Liver movement due to breathing is primarily influenced by the diaphragm's movement during breathing. The main movements of the liver are in the Superior-Inferior (SI) and Anterior-Posterior (AP) direction. The SI direction means toward the head(superior) and towards the feet(inferior) whilst the AP direction means toward the front of the body(anterior) and toward the back of the body(posterior). The current respiratory motion liver phantom that is used for research in the RAM group uses an

open-loop control scheme, in which a pattern is input for the SI and AP direction actuators. There are no sensors embedded into the system and the only ways of tracking the system to see if the reference signals are followed is by visually checking if the motion is correct, or by using electromagnetic trackers that are placed on the phantom liver that sits atop the respiratory motion stage.

1.2 Problem statement

The work done in this thesis is built upon the work of researchers who have developed a soft robotic phantom that simulates respiratory motion of a liver [5]. The main goal of this thesis is to make the setup more robust and realistic in terms of liver motion during respiration. From this main goal, the following objective was constructed:

- Create an MRI compatible realistic liver motion phantom to replicate movement in the SI and AP directions; 20 mm to 50 mm in the SI direction and 4 mm to 15 mm in the AP direction[6], [7]

1.3 Scope and limitations

The novelty of this thesis lies in making a fully MRI compatible anthropomorphic liver phantom, actuating it using pneumatic origami actuators. With this novelty as a guideline, the scope of this thesis will be focused on MRI-compatible design and Arduino controlled respiratory motion. Whilst every effort will be made to ensure that the re-designed stage is robust and stable as compared to the current phantom, there will be some limitations, namely with the materials used.

- **MRI-compatible design**: The main goal of this thesis is to develop an MRI-compatible liver phantom that mimics respiratory motion. The experiments and analyses that result from this phantom could then assist in planning needle insertion techniques for percutaneous liver biopsies.
- **Microcontroller-controlled respiratory motion**: The main objective of this part will be to reproduce human breathing motion in the form of sinusoidal signals given to a microcontroller (Arduino Uno) connected to pressure regulators. This form of human breathing motion is similar to patterns shown in previous research[8].
- **Materials used**: Since the motion stage has to be MRI-compatible, there are limitations in which materials can and cannot be used in the setup. The actuators have to be soft in terms of compliance which could result in faster wear and tear, as compared to electric or hydraulic actuators.

1.4 Scope and contributions of the thesis

The thesis will start with a Literature Review of current research setups used to mimic respiratory motion, particularly those that work in combination with a liver phantom. Afterwards, the design aspects of the newly developed phantom will be explained in the Design chapter. Snippets of Solidworks files will be found in this section. Following the Design section, the Methodology will be discussed. Actuator characterisations and experiments with sinusoidal breathing patterns similar to those shown in [8] will be talked about, and the Results of these experiments will be discussed to determine if the developed respiratory motion phantom accurately simulates the liver motion during breathing. Alongside the results, Discussion points will be stated. Lastly, a Conclusion and recommendations for Future Work will be presented.

2 Literature Review

2.1 Liver biopsy needle insertions

A percutaneous liver biopsy is a procedure where a needle is inserted into the skin and liver tissue is withdrawn to obtain a specimen to help in the diagnosis and treatment of various liver disorders. Given the advancements in imaging modalities such as Ultrasound, CT and MRI since the first invasive liver procedures, percutaneous liver biopsies can be targeted towards specific lesions to improve biopsy accuracy and decrease the rate of overall complications. A liver biopsy performed through a laparoscopic route is also an option, depending on the clinical context. However, the percutaneous route is generally the preferred approach. It is less invasive and less costly in comparison [9]. Overall, the evolution of the imaging modalities and the refinement of the biopsy methods have made percutaneous liver biopsies a staple in diagnoses and treatment of various liver diseases. As technology advances, it is likely that percutaneous liver procedures will continue to improve, solidifying their role in hepatology.

2.2 Soft actuator technologies

To be able to use phantoms inside MRI scanners, the entire phantom must be made up of non-ferromagnetic components. Most phantoms are therefore made up of 3D printed or laser cut plastic parts, with some non-ferromagnetic metals used to bolster the structure of said phantoms. In the case of a breathing simulation, there have to be some components that produce periodic motion on command. Pneumatic actuators are used for such purposes. They are MRI compatible, can be produced very easily, and are highly cost-effective for their purpose [4]. There are various types of pneumatic actuators such as linear and rotary pneumatic actuators, and each of these sub-divisions have various designs. For the purpose of this thesis, linear actuators will be used to simplify the motion of breathing in the SI and AP directions; specifically the pneumatic origami actuator developed by Mak et al [10]. The speciality of this study is that it makes use of various origami shapes such as the Kriesling and the cylindrical Miura, which allows the actuators to have unique mechanical properties. These actuators are also made using 3D printers which make them a quick and cost-effective solution for MRI compatible actuation.

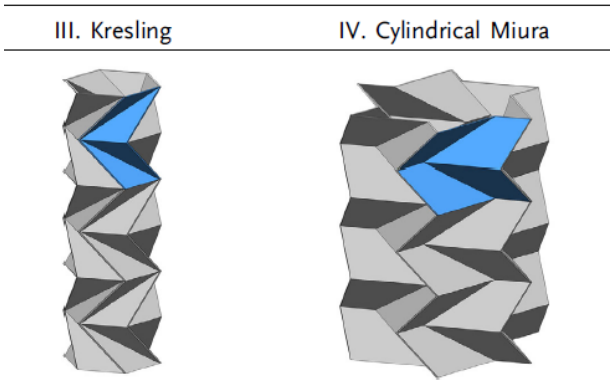

Figure 1: The Kresling and Cylindrical Miura shapes are what make up the structure of the pneumatic origami actuators [10]

2.3 Respiratory motion liver phantoms

A lot of research has been done on respiratory motion liver phantoms for various imaging modalities. Naghibi et al developed a robotic phantom that simulated respiratory motion of a liver with the help of pneumatic actuators that moved the phantom in the SI and AP directions, respectively [5]. This study focused on developing a phantom which could be used to improve the accuracy of hepatic tumor treatments. The developed phantom was fully MRI-compatible because it was made from lightweight 3D printed and laser-cut plastic parts. Soft pneumatic actuators were designed and implemented to achieve the respiratory motion in the SI and AP directions. This phantom is also capable of simulating different respiratory patterns with minimal movement errors. The system was thoroughly evaluated for repeatability and reliability through various cycle repetitions for different breathing modes. Some improvements to this phantom were made by Obbink [11]. Furthermore, this system was tested with patient-specific breathing patterns by inputting a different combination of the input parameters such as the input air pressure.

de Jong et al designed a PVA liver phantom that was used to simulate respiratory motion for needle-based interventions [12]. In this setup, a rib-cage and an abdominal phantom were also developed to make needle-insertions require a more realistic pathing towards the liver. Image segmentations from CT scans of real patients were used to measure the liver and rib displacement that led to the creation of the 3D-printed liver mold filled with PVA and the compliant rib cage. At the end, the liver phantom accurately replicated the respiratory liver motion and needle deflection observed in patients, thereby providing a useful tool for validating novel needle interventions. Ultrasound was the imaging modality of choice for this research because it is commonly used in abdominal procedures.

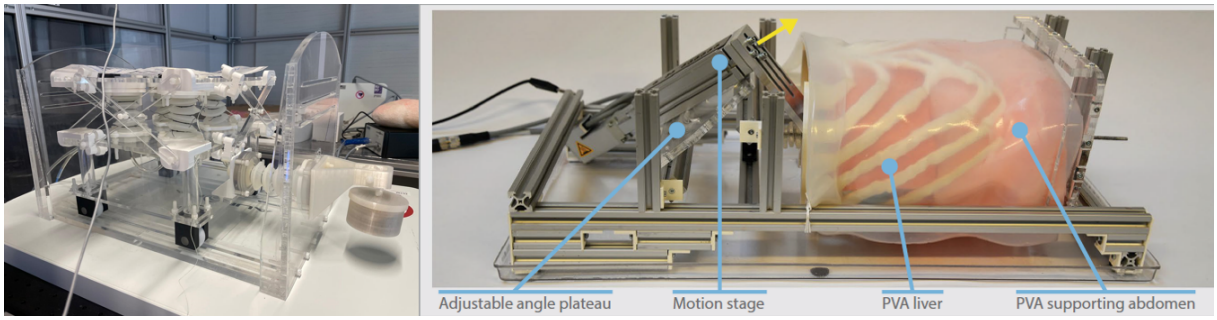

Figure 2: (Left) The previous respiratory motion phantom from the RAM lab at the University of Twente [11] (Right) PVA liver phantom developed by researchers at TU Delft [12]

2.4 Control

In the current robotic phantom setup that mimics respiratory motion of a liver, an open loop control scheme is used to produce the necessary motion [5], [11]. This means that there is no feedback from the system to determine if the appropriate displacements are made in the SI and AP directions, respectively. In an attempt to acquire more accurate movements, the Iterative Learning Controller (ILC) by Obbink [11] is used. The results of this study were promising; the setpoints of the position in the SI and AP directions were both reached with minimal error within a minute of the setup turning on. The actual pressure given by the air compressor was also extremely close to the reference pressure signal given by the controller on each iteration. Such a controller makes it useful to test various breathing patterns on the phantom setup so that biopsy procedures can be customised to be patient-specific, therefore creating a seamless experience for both the patient and the clinician.

3 Design of the phantom

This chapter describes the design process of the respiratory motion phantom and how the final design came to be. The first task that was performed during this phase of the project, was the functional analysis of the old liver phantom setup. With the results of this functional analysis, a set of features, requirements, and objectives were determined for the new respiratory motion phantom. Then the conceptualisation phase began with the drawing out of new configurations for the respiratory motion phantom. These concepts were then weighed up against one another, and re-iteratively updated until one design remained. During the conceptualisation phase, the requirements were continuously mapped to the design, resulting in design specifications for materials and components chosen. Since the actuation mechanism is arguably the most important part of the setup, there is a small subchapter on them. Lastly in this chapter, the challenges and limitations of the design process will be mentioned. The ultimate goal of this re-design was to make the liver phantom more realistic for needle insertion procedures and modular so that broken parts can be repaired/replaced easily.

3.1 Functional analysis

A functional analysis was performed on the older liver phantom setup to determine which components were important and which would be excluded in future iterations of the setup. To do this, the following steps had been taken:

- ***System definition and identification of components*** - In this step, the old system was defined by its basic movement functions and what the setup was used for, namely, the liver phantom that sits on top moving in the SI and AP directions, and that this phantom setup was used for needle insertion procedure testing.
- ***Interaction and function mapping*** - It is important to map out the relationships between the components to understand their interfaces and how they interact with each other. Using the information from the first step, a diagram of the components and how they interact with each other was made and can be found in the Appendix in Figure 22.
- ***Evaluating the performance of the current phantom*** - The actuation mechanism of the current liver phantom achieved the necessary motion required in the SI and AP directions of liver motion, thereby allowing liver movement patterns to be accurately portrayed. However, some of the components are cumbersome and inefficient and need to be adjusted several times during the experimentation period. The scissor lifts of the set-up, as seen in Figure 2 come out frequently and need to be placed back onto the flat plates for the setup to work again. The rubber actuators also seen in Figure 2 often leak and need to be repaired with plastic twine or replaced altogether.
- ***Determining failure modes of old setup*** - The results of this section can be seen in the bullet point above. The main causes of failure of the system were the scissor linkages and the rubber actuators.
- ***Defining features, requirements and objectives for new setup*** - After analysing the old setup to see which components were to be replaced/removed, a set of features, requirements and objectives were written out for the future setup. These can be seen in Table 1 below.

Table 1: Requirements, features and objectives of the re-designed phantom

Requirements	Features	Objectives
MRI compatible	Realistically shaped liver	Portray liver motion due to breathing
Withstand needle insertion forces (maximum about 0.65N) [13]	Visibility to researcher	Can be used for MRI experiments
Breathing motion replication (SI motion between 20-50 mm and AP motion of maximum 15 mm [6], [7])	Realistic needle insertion boundaries	Can be used for needle insertions procedures
Modular	Ease of Maintainability	Can be used for motion compensation experiments
Complies with MRI safety standards	Simple Functionality	
The liver phantom should be visible under MRI	Optimised for Manufacturability	
Entire setup fits inside an MRI bore (60-70cm)		

3.2 Conceptualisation

With the results of the functional analysis, the conceptualisation phase could begin. The main steps involved in this phase were drawing sketches of concepts, discussions with supervisors for feedback on designs, and selection of concepts based on the requirements found in the functional analysis. Initially, the thesis was meant to improve on the current liver phantom so as to have a seamless integration of the new device with the current codes. However, as the thesis developed, the need for a more realistic phantom arose, to allow for more real-life needle insertion procedures to be simulated. One of the ideas was to take into account liver deformation by allowing it to push up against a barrier. Another idea was to add various organs to make it a holistic organ phantom instead of only focusing on the liver. Some sketches of concepts can be seen in Appendix A below. Explanations of why each phantom was not chosen are written underneath each figure. After various iterations and discussions, it was decided to fixate on the design shown below in Figure 3. This design fulfilled the requirements from Table 1 without extra complicated components.

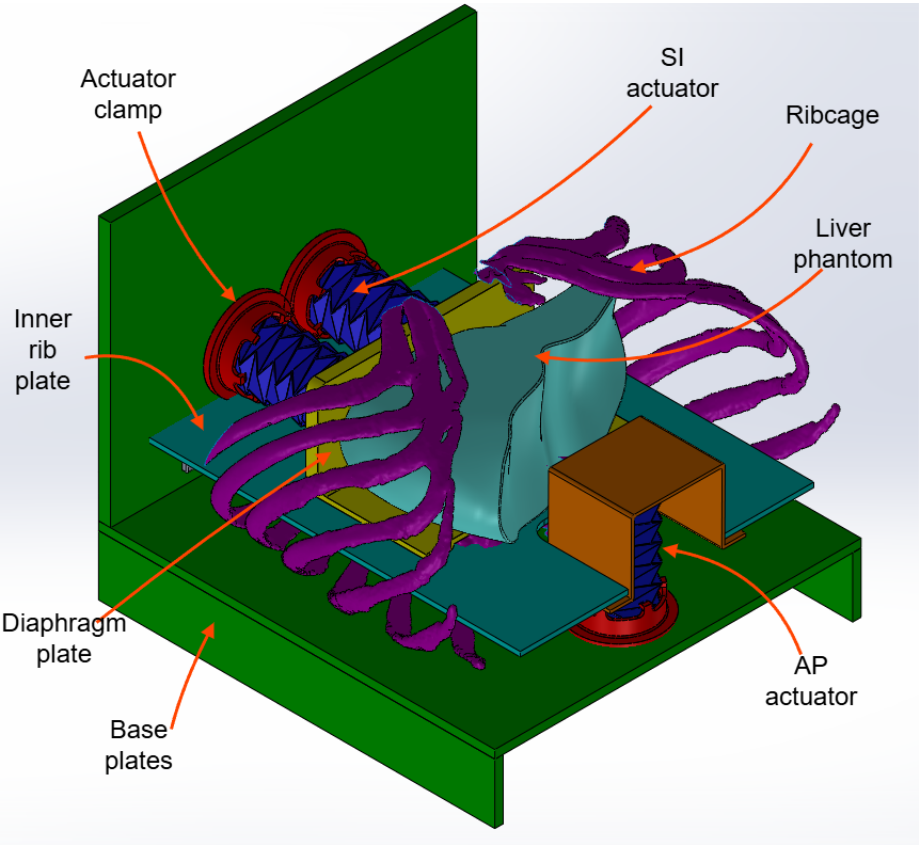

Figure 3: A Solidworks model of the redesigned liver motion phantom

3.3 Design specifications

The design specifications were chosen by looking at the requirements and seeing how those would fit seamlessly as part of the final concept. A mind map of the design specifications can be seen below in Figure 4.

Dimensionally, only 2 specifications were made; that the liver phantom should have a realistic shape so as to accurately represent the boundaries of the human organ, and that the overall size of the newly developed liver phantom setup should fit into the MRI-bore. These specifications were made to make sure that the new setup was easily portable for use in various experiments in different locations. The span of the liver is 11-12 cm in males along the midclavicular line, which is the longest vertical edge of the liver [14]. The current liver phantom at the RAM lab matches this constraint and can therefore be used for this thesis.

For the choice of materials, the main requirement was that the setup should be made of non-ferromagnetic materials, to allow researchers to be able to use this setup with MRI technologies. Another requirement was that the setup should be made with cost-effective components. As a result of these requirements, laser cut plastics were used for the base and structure, 3D printed parts for the actuation mechanism and ribcage, and an already existing liver phantom made out of rubber was used, ensuring both cost-effectiveness and MRI compatibility.

For functional requirements, four different specifications were chosen as key. The modularity of the components was important so that adjustments could be easily made and so that parts could be removed/replaced with ease in the event of breakage or need of repair. Compatibility with MRI technologies is important as stated before. Motion control is key because the main purpose of this setup is that analyses can be done on the motion of the liver due to respiration. Movements of the liver

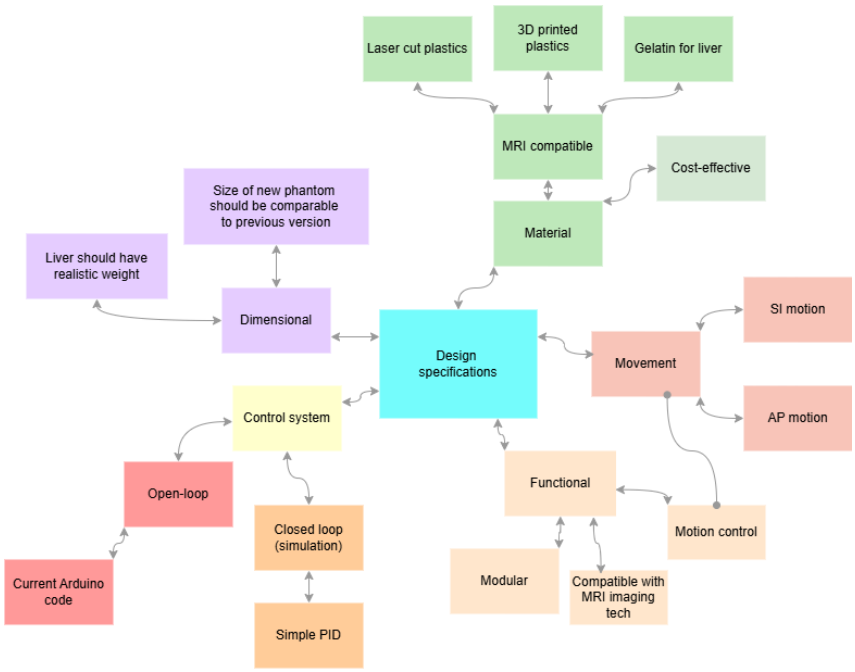

Figure 4: Mind map of the design specifications

phantom happen only in the SI and AP directions, as these are the main movements of the liver inside the human body. The movement of the liver in the left-right (LR) direction is neglected because it has a negligible magnitude in comparison to the other two (< 5 mm) [15].

The requirements for the control system were two-fold. The open-loop system was used for the validation of the newly developed setup. The open-loop code allows pneumatic pressure to be input into the actuators with a fixed magnitude in the SI and AP directions. The closed loop controller will make use of electromagnetic (EM) trackers to acquire position data of the liver phantom. Although EM trackers will be employed to acquire the position data of the phantom in the current study, they will not be utilized in the MRI environment due to interference caused by the magnetic field generator, which impedes the functionality of the EM tracker sensors. This position data will then be relayed through the Arduino board to the MATLAB/Simulink model. The controller will then compensate any errors in position from the reference input signal to the actual output of the liver phantom.

From the aforementioned design specifications, it can be said that the newly developed phantom setup possesses the following *system qualities*:

- ***Simple functionality*** - to make the system in such a way that allows the liver to move in both the SI and AP directions with as few components possible to realise these motions.
- ***Ease of maintainability*** - done by making most of the system modular. The actuators are stuck inside the clamps with a friction fit instead of being stuck together with glue. Most of the components slot within each other and are not rigidly attached to one another; hence, they can be easily removed from the system and replaced in the case that the parts get damaged and need repairing.
- ***Optimised for manufacturability*** - done by having most of the parts being 3D printed; hence the components only use one manufacturing process, and a relatively low cost one at that. Parts can be easily reproduced if needed. Furthermore, the base of the structure is made of laser cut plates.

With all these requirements and specifications in mind, several concepts were thought out. The final concept is shown in subsection 3.2 above in Figure 3, and an explanation of the components and their interactions is presented below. Some sub-assemblies of the components can be seen in Appendix B below.

Components and their interactions

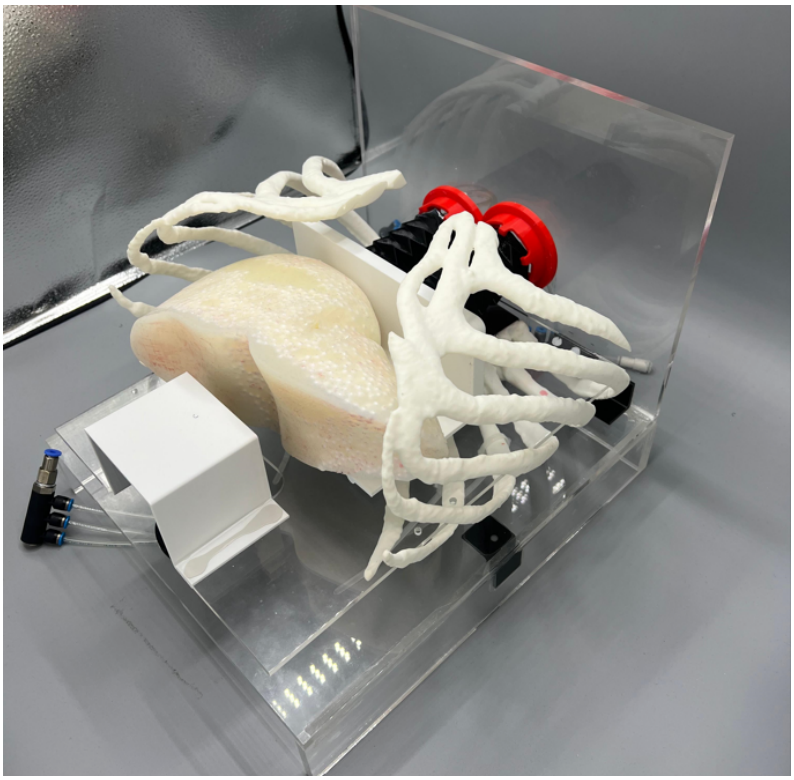

Figure 5: Isometric view of the liver phantom

All the components can be seen in Figure 3 and an image of the realised setup can be seen in Figure 5. The base plates are the fixed structure of the respiratory motion cart. The actuator clamps are fixed into holes that are laser-cut into the base plates and they are kept in place using Bluetack adhesive putty. The SI actuators and AP actuator sit inside their own actuator clamps. The actuators [10] can "twist and lock" into the clamps because of the snap-fit joints placed on the upper ring of the clamps. The SI actuators push up against the diaphragm plate due to the positive air pressure given to them by 4 mm pneumatic tubes. There are 2 cavities on the diaphragm plate in the shape of the top actuator face that make sure that the actuators do not slide around and produce rotation in the SI direction; only translation. On top of this diaphragm plate sits the liver phantom, which is the primary subject of the motion, as well as the main target for needle insertion procedures. The liver phantom is made by pouring rubber into a mold and dispersing styrofoam balls throughout the phantom. The use of the styrofoam balls is to make sure that the phantom is light. The ribcage was 3D printed using the Selective Laser Sintering (SLS) method and forms the boundaries for needle insertions. Connected through hinges on the back base plate, is the inner rib plate which sits on top of the ribcage. This inner rib plate has a shelf for the AP actuator at the opposite side of the hinged edges, which allows the AP movement to be produced. As can be seen in Figure 5, along the inner side of the base plates and on the back wall of the base structure are 3D printed L supports which are glued to the base using Araldite two-component glue to bolster the structural integrity of the base.

3.4 Origami actuators

The origami actuators were designed by Yoeko et al [10]. They can be seen in Figure 6b below. A Solidworks model of the actuator can be seen in Figure 6a below as well. In their research, TPU95A (shore hardness 95A) was used as the material for the actuators. However, in this research, TPU92A (shore hardness 92A) was used because it is a softer material, with similar pressure-to-force capabilities. Origami actuators such as these are inherently compliant. This compliancy can be defined in various ways. One relevant way to describe this compliancy is to determine the stiffness of the actuators. For simplicity of calculations, these actuators were assumed to have spring-like behaviour for the experiments. Characterisation experiments of these actuators were done to determine their stiffness, extension under pressure and force production capabilities. These experiments are explained in section 4.

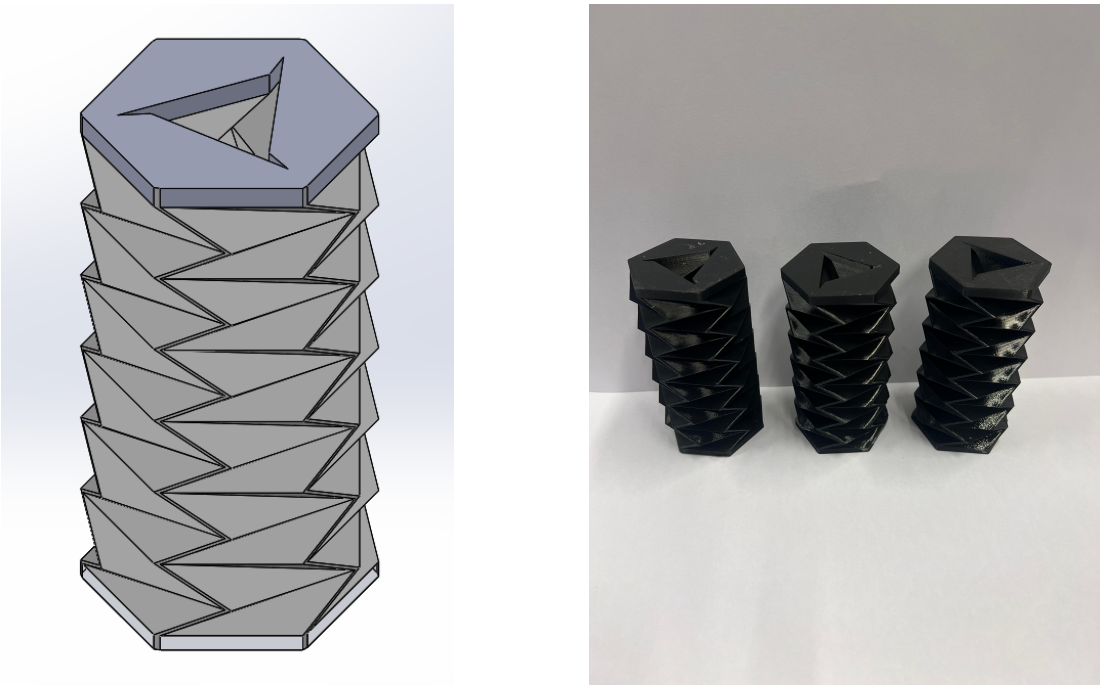

(a) **(b)**

Figure 6: (a) The Solidworks model of the pneumatic origami actuator (b) Three 3D printed origami actuators made from TPU92A.

It cannot be seen from Figure 5, but in the physical setup, when the SI actuators are fitted to the diaphragm plate in their rest position, there is a slight bend of the actuators along their lateral axis. This slight deflection was calculated, to see if it would have any impact on the force output of the actuators. For ease of calculation, the actuators were assumed to be cantilever beams fixed on one end, and having a point load on the other end, causing a bend in the "beam". An image of the approximation can be seen in Figure 7a below.

The following formula was used to calculate the deflection:

$$\delta_{\max} = \frac{PL^3}{3EI} \tag{1}$$

where P is the weight of the point load in newtons (N), L is the length of the beam in millimetres (mm), E is the modulus of elasticity in megapascals (MPa) and I is the area moment of inertia in mm^4. P was taken to be 0.564 N half of the weight of the diaphragm plate, as this was the point load that caused the bending of the actuators, and it was halved because there are two actuators connected to the diaphragm plate. L was the length of the actuators which is 96 mm. E was given in a datasheet of

TPU92A as 90 MPa [16] and I was calculated to be 1000000 mm^4. By substituting these values into Equation 1, the resulting deflection is calculated to be **0.00185 mm**. This value can be considered negligible due to it's extremely small magnitude, even when compared to the actuator's inner wall thicknesses of 0.6 mm [10]. Furthermore, this deflection introduces an insignificant variation in the force calculation, whether the force is applied directly or with a deviation of 0.00185 mm. A simulation of the cantilever deflection was also done in ANSYS to verify the approximated hand calculation and the result can be seen in Figure 7b below. The red arrow represents the point load P.

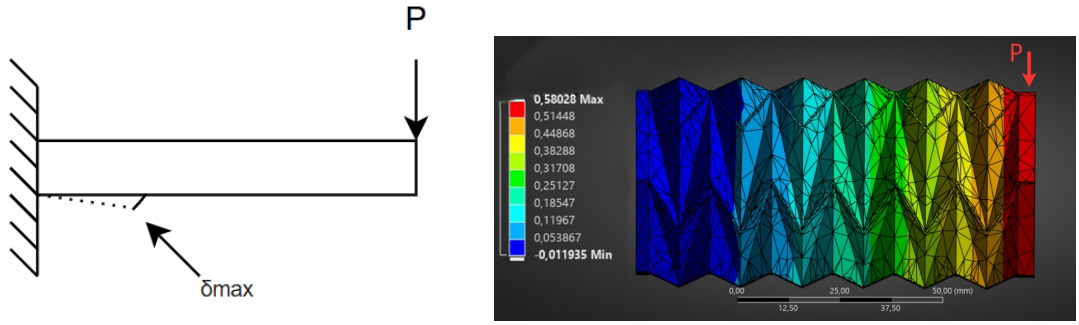

(a) **(b)**

Figure 7: (a) Simplified approximation of the SI actuator as a cantilever beam; fixed on one end with a point load P on the free end resulting in a deflection of δ_{max} (b) ANSYS simulation of the SI actuator as a cantilever beam showing maximum deflection of 0.58 mm.

The result of the ANSYS simulation shows a deflection of 0.58 mm at the free end of the actuator, which is considerably higher than the deflection predicted by the hand calculation. This difference comes about because the FEM analysis accurately models the complex geometries of the actuator, whereas the hand calculation simplifies the actuator to an idealized rectangular cantilever beam, thereby neglecting shape-specific characteristics that influence deformation of the actuator. However, this deflection is also still not enough to cause a significant variation in the force produced by the actuator. Therefore, this deflection can be truly regarded as insignificant, and no changes have to be made to the design to account for this deformation.

3.5 Challenges and limitations

Some of the challenges and limitations met during the design phase are mentioned in the list below.

- The origami actuators were 3D printed, and since the 3D printers are never perfect, every actuator that was printed came with at least 2 minor leaks and 1 major leak that resulted in significant pressure loss in the respective chamber. The leaks were closed up in two ways: using the two-component glue Araldite and using a liquid TPU sealant. It is commonly known that the best material to coat TPU is TPU itself. Therefore, the TPU sealant was acquired. However, this sealant is liquid and is difficult to apply to all the leaks due to the geometries of the actuators, and it takes over 27 hours to cure completely. Furthermore, after complete curing of the sealant, the closed up leaks tore open again after 30 cycles of actuation. Ultimately, it was decided to use the Araldite glue to close up the leaks, which sealed the leaks quite well. However, it did increase the stiffness of the certain folds of the actuator on which the glue was applied. This could have an effect on the performance of the actuators, but could be considered negligible since it is not an extremely high-precision application.

  Another attempt was made to close up the leaks by coating the actuators in Formlabs elastic 50A resin [17] and curing it in an ultra-violet light oven at 50°C for 20 minutes. However, just

after one actuation cycle, the coating stripped off the actuator. An image of the actuator with the coating can be seen in the Appendix in Figure 23

- Initially, using the two-component glue to bind acrylic plates together for the base was done. However, this was not a permanent solution. The components were constantly falling apart every couple of weeks due to the loss of adhesion. Ultimately, this was fixed with the use of 3D printed supports that were used to reinforce the base plates. Other parts, like the hinges of the base plate were screwed onto the acrylic plates to ensure that they maintained their position in the liver phantom setup.

4 Methodology

In this chapter, the methods and experiments used to validate the physical system are explained. At the end of this section, an explanation of the closed loop controller that was developed in 20-sim is provided.

4.1 Actuator characterisation

For the force-length and pressure-length characterisations, the software Tracker [18] was used for the analysis. An image of the Tracker software can be seen in Appendix A. Videos were recorded on an iPhone 13 Pro that was placed in a clamp, so that movement from the camera would not be a factor in the results of the analysis. Calibration of the software is done using a ruler on the side of the actuators as seen in Figure 8a and Figure 8b. A small marker was used as the reference point for the software to detect tracking movements of the actuator. These markers were chosen for their size and visibility in Tracker. For each experiment below, three readings were taken per actuator, with a total of three actuators tested. Hence, each experiment has nine datasets, providing reliable datasets to characterize these actuators. For all experiments, the actuators were placed in an actuator clamp on top of a 3D printed stand, to make sure that they were fixed in place and remained upright throughout all experiments.

4.1.1 Pressure length characterisation

The first set of experiments done was the pressure-length characterisation. The setup is seen in Figure 8a below. Air pressure was fed into the three chambers of the actuator using a 3-way connector from FESTO [19]. The pressure regulator **VPPE-3-1-1/8-2-010-E1** from FESTO only outputs a maximum of 2 bar and was used for this setup. Hence, the actuator characterisations were done from 0 to 2 bar in steps of 0.25 bar. The pressure steps were fed into the actuators three times for each of the three actuators, resulting in nine datasets. The same was done with a vacuum generator to see how much the actuator would compress given different vacuum steps. The vacuum generator produced vacuum pressures from -0.1 bar upto approximately -0.4 bar. Tracker was used to track the extension of the actuator due to the input air pressure. The results of these experiments are explained in the Results section below.

4.1.2 Compression length characterisation

The setup for this experimental condition was similar to the pressure-length characterisation but it had various masses sitting on top of the actuators. A picture of the experimental setup is shown in Figure 8b. Weights of various magnitudes were then placed on top of the actuator to force the actuator to compress. The weights used were 100 g, 200 g, 300 g, 500 g, 600 g, 700 g and 1000 g. The initial starting length of the actuators were all measured to be 95 mm. A potential source of error in this experiment is that once the weight increased to 500 g and above, the weights had to be held on top of the actuator to prevent them from falling over and destroying the equipment. This introduces uneven force distribution as the human hand cannot hold the weight perfectly still. However, this compromise does not significantly impact the results as the impact of any "extra" forces introduced by the hand would not cause any extra deformation of the actuator itself.

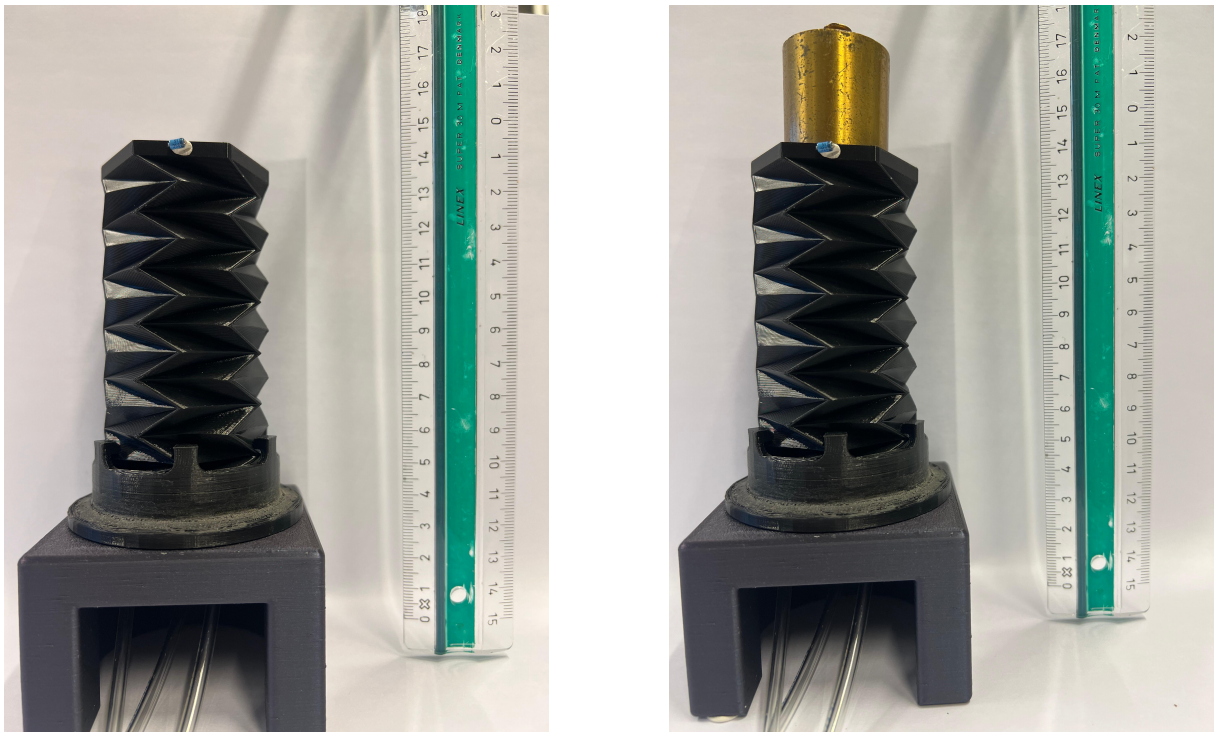

(a) **(b)**

Figure 8: (a) Actuator connected to pneumatic tubes with a ruler on the side to calibrate Tracker when measuring the extension of the actuator due to input pressure (b) 200g weight placed on top of the actuator to measure the compression of the actuator. Various weights were placed on top and no air pressure was input for these experiments

4.1.3 Pressure force characterisation

For these set of experiments, the same setup was used as that of the pressure-length characterisation, but with the addition of a force sensor placed on top of the actuator. The setup is seen in Figure 9a below. The force sensor used was a TAL220 10 kg sensor that interfaces with an Arduino board using an HX711 load cell amplifier. The force sensor converts the analogue signals from the actuator pushing up against it into digital signals that are output as kilograms in the Arduino serial monitor. The weights that are output into Arduino are then converted into force values by multiplying them with gravity (9.81 m/s^2).

During these experiments, it was noticed that buckling occurred at 1.25 bar air pressure and above as seen in Figure 9b below. This phenomenon could be due to a variety of reasons such as uneven air leakages in the actuators, imperfect placement of the load sensor or uneven print surfaces on the inner layers of the actuator itself. To fix this issue to allow for better force readings, a tube with one small section open was 3D printed and fit around the actuator whilst being placed on the actuator clamps with BlueTack so that it would stay put. An image of the revised setup can be seen in Figure 9c below. This improved the reliability of the readings since the actuator had nowhere to push but upwards directly onto the force sensor.

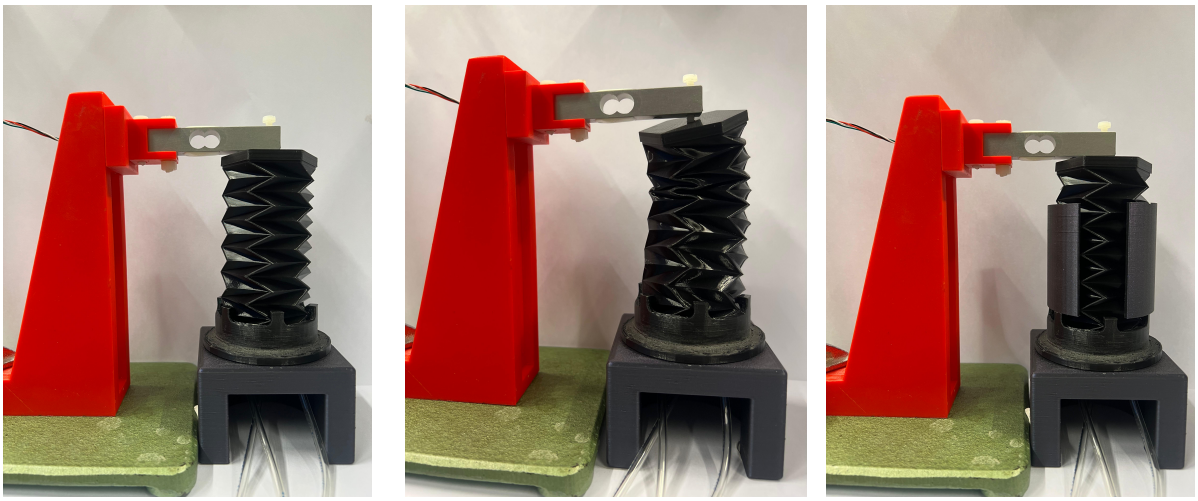

(a) **(b)** **(c)**

Figure 9: Experimental setups: (a) Load cell sensor mounted on top of an origami actuator to measure actuator forces produced due to input air pressure , (b) Origami actuator buckling due to high input air pressure of > 1.25 bar, (c) Improved setup with 3D printed tube that reduces buckling of the actuators when measuring forces

4.2 Validation with open loop code

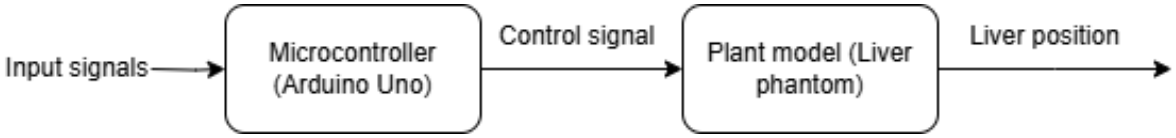

Figure 10: General schematic of an open-loop control system

A schematic of an open-loop control scheme can be seen in Figure 10. The air compressor, Arduino and pressure regulators used to produce air pressure can be seen in Figure 11 below, along with a schematic of the components together. A sinusoidal input was given to the Arduino so that the regulators could provide the corresponding air pressures. Results of this experiment are seen in the section below.

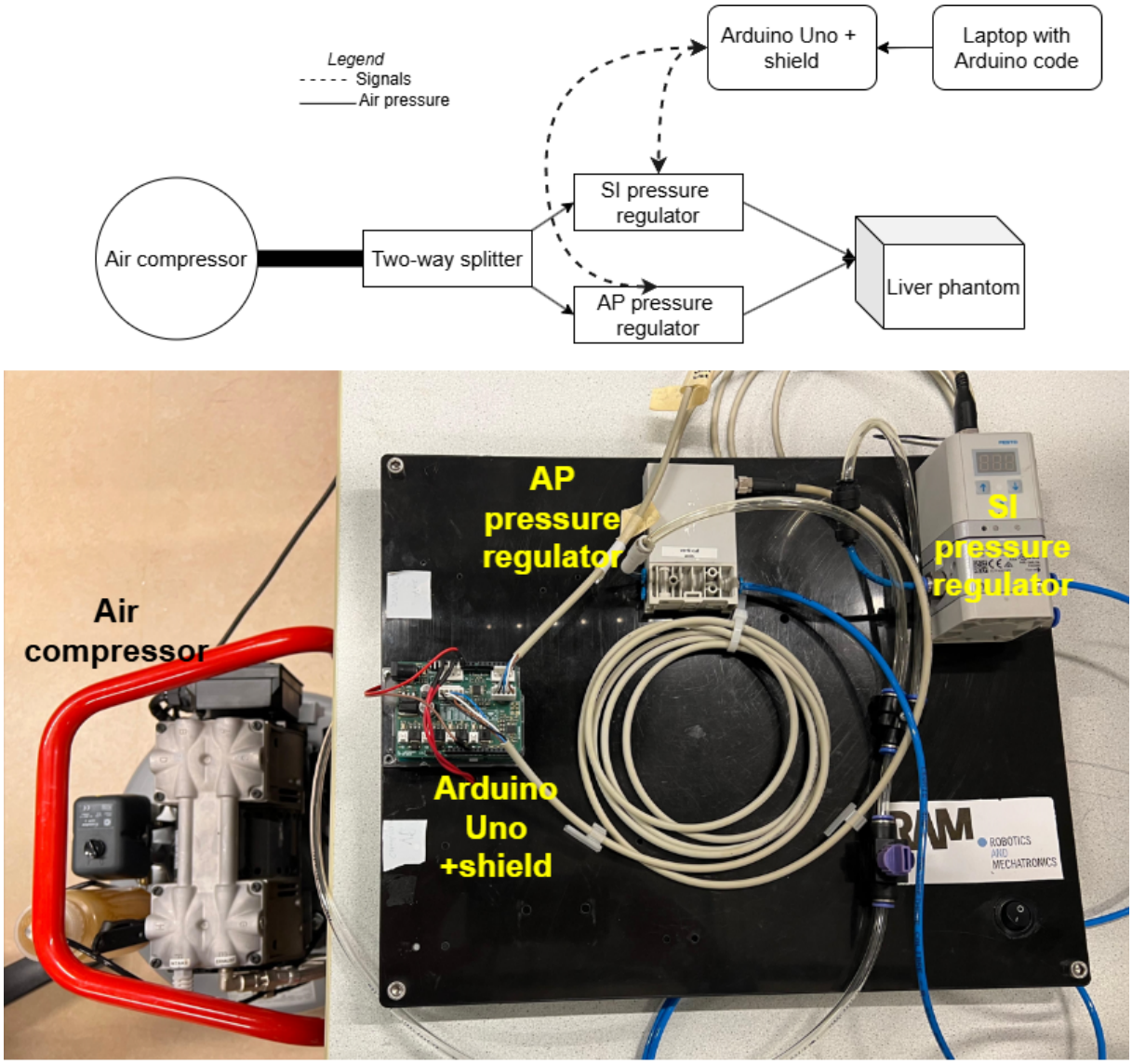

Figure 11: Schematic of an Arduino board and pressure regulators connected to an air compressor and an image of the physical components from the schematic

4.3 Closed loop controller

A simple PID controller was developed in 20-sim with an idealistic model of the physical setup. It can be seen in Figure 12 below. This model is representative of the SI actuators, as these are the actuators that have a greater range of motion and need to be fine-tuned to produce more accurate breathing motions.

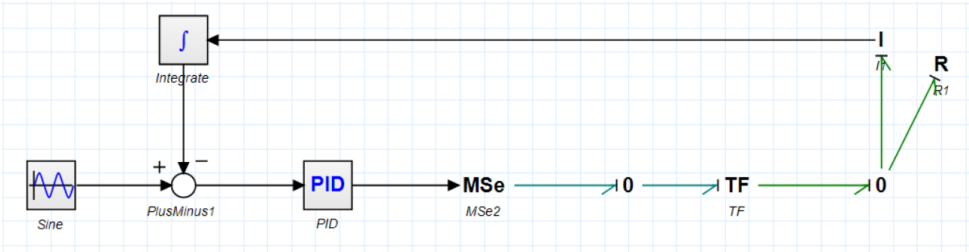

Figure 12: Model of the SI actuators in 20-sim with a feedback loop into a PID controller

The system is actuated using a Modulated Effort Source (MSe) element to represent the varying sinusoidal input of air pressure into the system. "0 junctions" are used to represent that the effort of the air compressor is continuous across the whole system. A Transformer (TF) element is used to transform the setup components from the pneumatic domain to the mechanical translational domain. The Inertia (I) element and the Resistance (R) element on the right side are used to represent the mass that the actuators push up against, and the very little friction that is present in the physical system. The output of the I element is a flow, which means that the output of the I element is the velocity of the mass that the actuators push. Hence, this output is integrated to acquire the position of the mass, and the result of the integration is fed into a sum block, along with the reference signal, to produce an output. This output of the sum block is the system error, which is the difference in position of the mass from where the reference says it should be, to where it actually is. This signal is then fed into the PID controller in hopes that the error can be minimised so that the system follows it's reference signal. The heuristic method of trial and error was used to tune the PID gains for this system. The closed loop transfer function of the system was calculated by using the Model Linearization toolbox in 20-sim where the *input* was taken as the output of the Sine block (the reference signal) and the *output* was the output of the Integrator block (mass position). The closed loop transfer function of the system is as follows:

$$\mathrm{TF} = \frac{output}{input} = \frac{400s^2 + 293.3s + 53.33}{s^4 + 6.667s^3 + 400s^2 + 293.3s + 53.33} \tag{2}$$

5 Results and Discussion

In this section the results of the experimental setups in the section above will be discussed. Tracker and MATLAB were used to analyse the data of the experiments.

5.1 Actuator characterisation

In this subsection the results of the actuator characterisation experiments will be explained. Raw data from the experiments was plotted into graphs and those can be found in Appendix C.

5.1.1 Pressure length characterisation

The aim of this experiment was to determine how far the actuator could extend, given input air pressure from 0 to 2 bar. The results of this experiment can be seen in Figure 13 below.

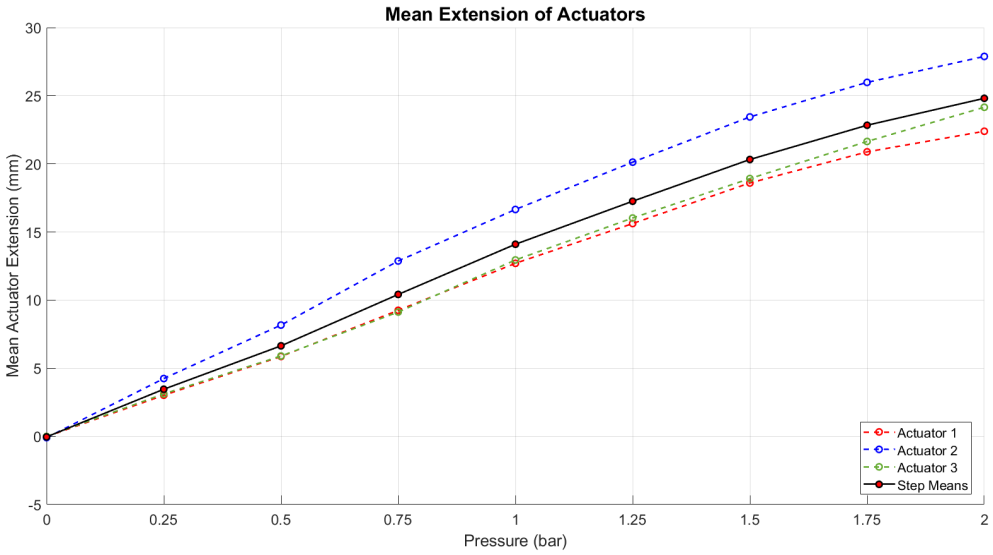

Figure 13: Average extensions of the actuators with input pressure from 0 to 2 bar

Looking at the resulting graph, a near-linear relationship is seen, which indicates a proportional relationship between positive pressure and actuator extension length within the range of 2 bar. This confirms that the actuators can reliably reproduce the required ranges of motion needed to replicate human breathing. The average maximum extension that the actuator achieves at 2 bar is ≈ 25mm. This shows that the actuator can behave predictably given varying pressures.

The actuators were also tested with vacuum input pressure from -0.1 bar to approximately -0.4 bar. The results of the experiments are shown below in Figure 14. The average maximum compression of the actuator from rest position is ≈ 27mm. This graph also shows a near-linear trend between vacuum pressure and the actuator compression length. The actuator was meant to be tested upto ≈ -1 bar, but due to malfunction of the equipment, only tests upto -0.4 bar could be done. These experiments prove that the actuator can indeed satisfy the requirement of the ranges of motion as mentioned in the Requirements in Table 1.

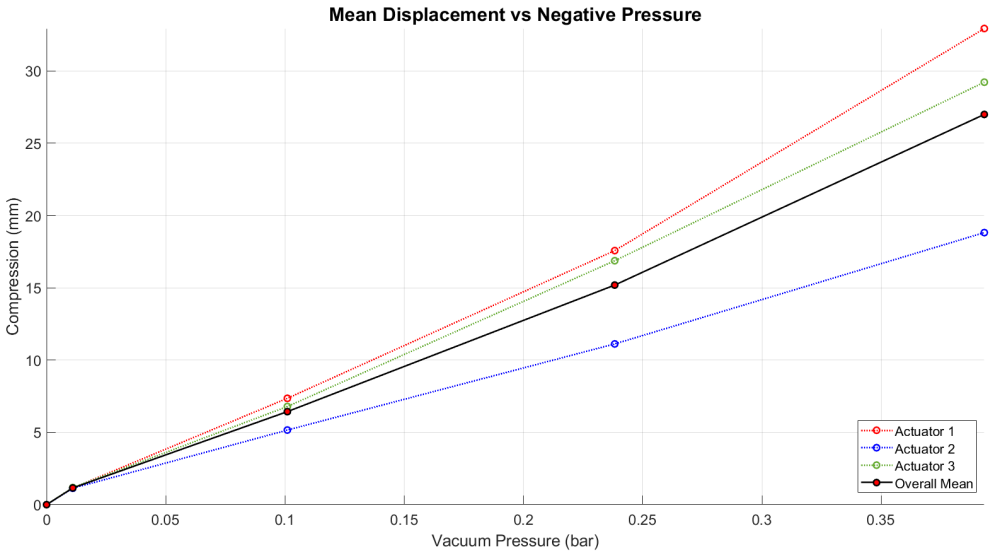

Figure 14: Average displacements of the actuators with input vacuum pressure from 0 to -0.4 bar

5.1.2 Compression length characterisation

The objective of the experiment was to analyse the compression behaviour of the actuators under varying weights. The results of the experiment are seen in Figure 15 below.

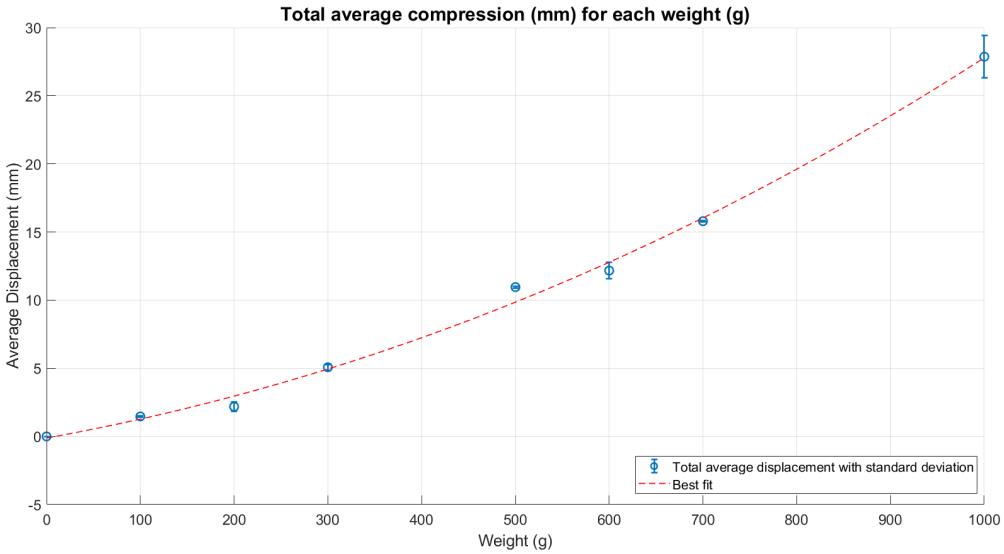

Figure 15: Average compression of the actuators vs weight placed on top of the actuators

Looking at the graph, a non-linear stiffness relationship between the weight and the displacement is seen, as shown by the best fit cubic polynomial. However, this non-linearity does not come into play for the motion of the phantom. The standard deviation of the readings of three experiments per actuator for all three actuators is relatively low. However, at 1000 g there is a notable increase of the deviation, indicating greater variability at higher loads. This most likely comes as a result of the experiment method of holding heavier weights with the hand on top of the actuator itself.

5.1.3 Pressure force characterisation

The final actuator characterization was conducted to determine the output forces generated by the actuator in response to varying air pressures, in the range of 0 to 2 bars. The results of the experiment can be seen in Figure 16 below.

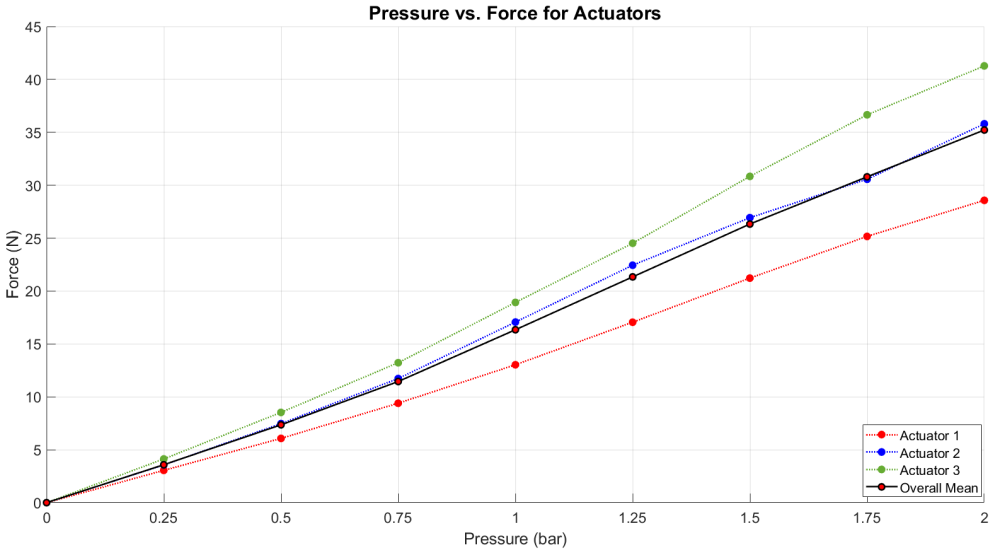

Figure 16: Average force output of the actuators due to input pressure from 0 to 2 bar

The maximum average force produced by the actuators at a pressure of 2 bar is 35N. This means that the AP actuator can produce enough force to lift up the weight of even the heaviest liver phantoms that could be placed in the setup [14]. Looking at the average of all three actuators the relationship between the pressure and force looks to be approximately linear within the tested range. The variability of the readings seems to increase at higher pressure levels, which could be attributed to the limitations of the sensor because a slight drift was noticed in the sensor readings. It could also be due to leaks in various places of the actuators. Most of them had been sealed with Araldite glue but re-open after about 100 cycles. For future experiments, the range of pressures can be increased to see if the linear pressure-force behaviour remains.

5.2 Open loop experiments

The results of the open loop validation experiments will be explained in this subsection. The open-loop experiments were done only for the positive pressure range due to constraints of the available equipment. For the open-loop experiments Tracker [18] was once again used to track the movement of the liver in the SI and AP motions.

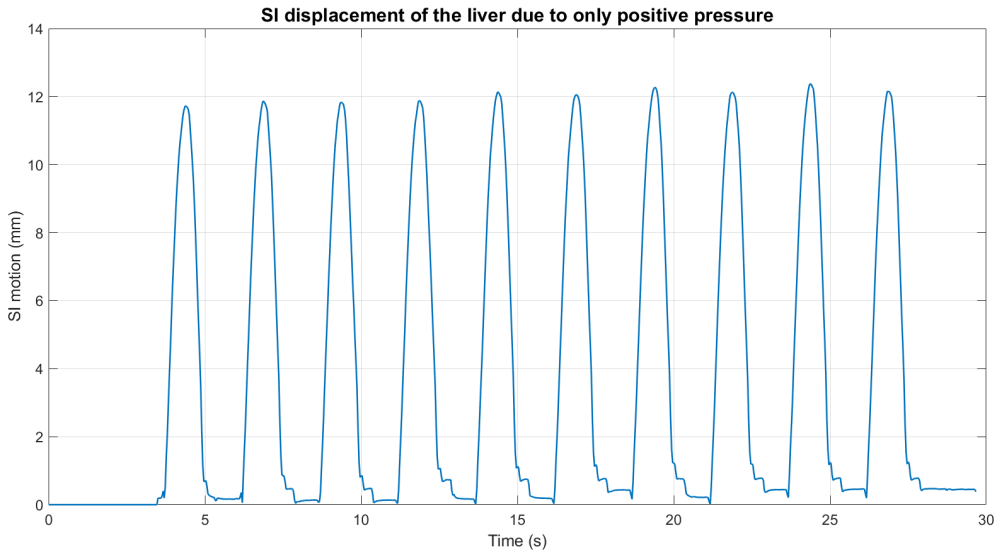

Figure 17: Sinusoidal motion of the liver in the SI direction

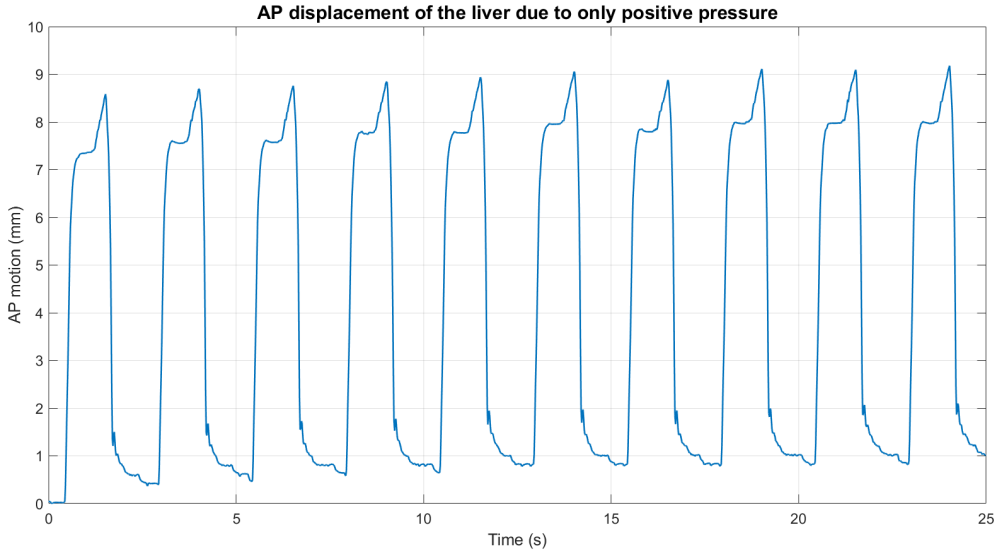

Figure 18: Sinusoidal motion of the liver in the AP direction with small bumps at each peak

Looking at the graphs, the liver motion in the SI direction is smooth and periodic with consistent peaks and valleys across the measured timespan. An average motion of 12 mm is achieved in the SI direction. Taking a look at the AP motion of the liver, it is less smooth and has a little bump before each peak in the measured timespan. An average motion of 8.75mm is achieved in the AP direction. The small bumps can be attributed to the pressure regulator that is used for the AP direction, which contributes to the abrupt motion of the AP movement. The current regulator in the AP direction makes a high pitched noise when it is activated every cycle, meaning that there are pneumatic oscillations within that cause the abruptness of the air output. For further experiments, a different pressure regulator should be used for the AP direction. Smoothing of the input signal to the AP regulator was attempted, however it did not change the output significantly.

There were some other limiting factors for the movement of the actuators such as the FESTO pressure regulator only producing 2 bars, which then gets split between 2 actuators, essentially giving only half

the necessary input air flow to each of the SI actuators. Hence, a regulator with more air pressure range could be useful for further experiments. The pneumatic origami actuators are also prone to leaks which affect the performance. The issue was partially addressed using a two-component glue, but further research into more robust actuator materials or a different manufacturing method is needed.

A combination of a vacuum pump and an air compressor would also help increase the range of motion needed to fulfil the motion requirements. When both the positive and negative lines of pressure were tested with the available equipment, the range of motion did not change due to the residual air in the pneumatic lines that the vacuum had to overcome in order to compress the actuators. A potential solution to this would be to have an electronically controlled two-way splitter that takes signals from the microcontroller and switches between a positive and negative pressure line. This way there will be dedicated pneumatic lines for the air compressor and vacuum, but the vacuum won't have to overcome any residual air before compressing the actuator. Moreover, while the open-loop system successfully reproduced sinusoidal motion to represent breathing, there is no feedback in the system. Therefore, the precision of the phantom's movements is limited.

5.3 Closed loop simulation experiments

From the model shown in Figure 12 above the following simulation results were acquired. The reference sinusoidal signal and the actual mass position are shown in Figure 19 and the position error between the two are shown in Figure 20. Using relationships that mapped the pressure-length of the actuators to the input Sine Block in 20-sim, the output of the displacements moved by the mass were given. The error shoots up in the first second but quickly stabilises afterwards to a steady-state error of just above 0.1 mm. The initial error of the system with untuned PID gains were of the order of 1 mm, but with some tuning of the parameters, a much lower steady state error was acquired. Although these are the results of an idealistic model, this shows that there is potential for a closed loop controller to make the system reproduce breathing motion in a more accurate way. Integrating a more complex closed loop controller that takes into account the non-linearities of the system, with a better microcontroller would allow for more accurate representations of human breathing.

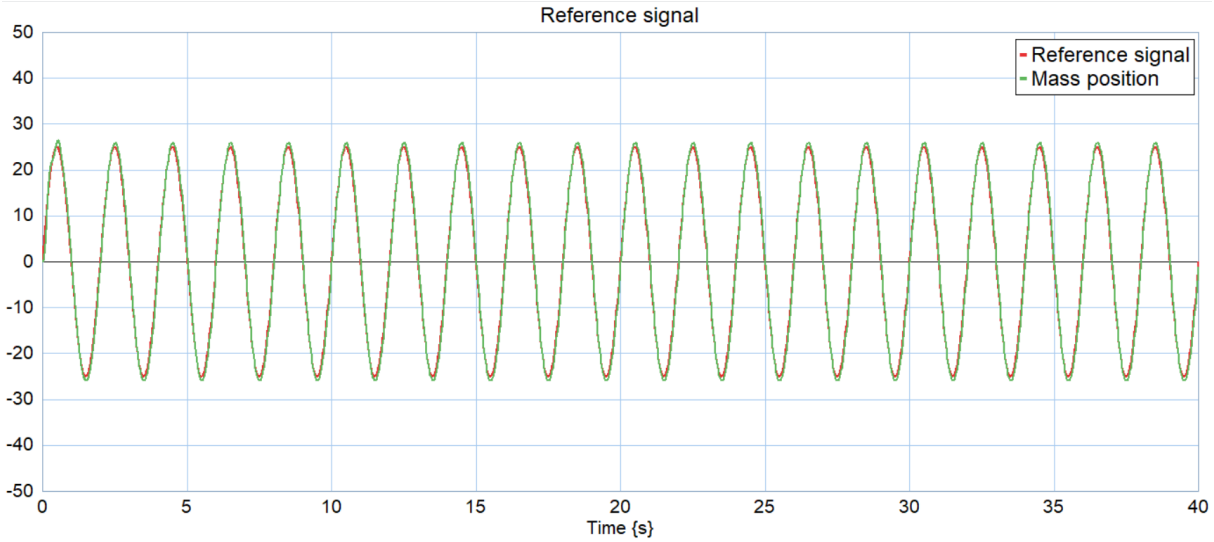

Figure 19: Input reference signal vs actual position of mass

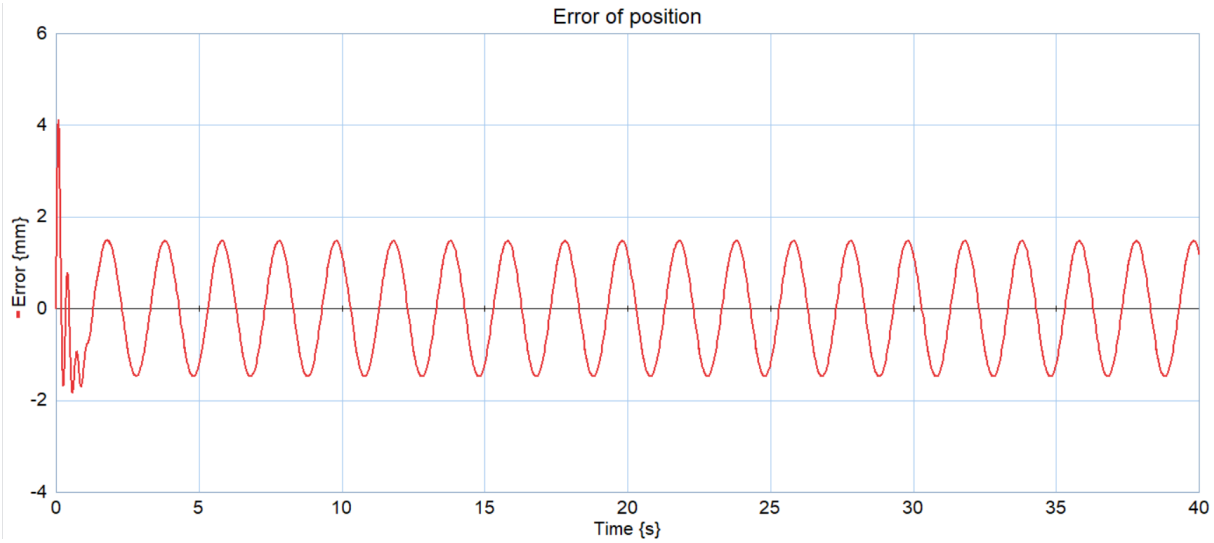

Figure 20: Position error from the difference of the actual position of mass and the input reference signal

6 Conclusion and Future work

Conclusion

The development of an MRI-compatible anthropomorphic liver phantom is presented in this thesis and marks a step forward in the field of medical imaging and surgical robotics. This liver phantom setup makes use of pneumatic origami actuators which are lightweight, cost-effective, MRI compatible and can repeatedly be produced fairly quickly. The phantom successfully replicates respiratory-induced motion in both the SI and AP directions; 12 mm in the SI direction and 8.75 mm in the AP direction. The modular design ensures functionality and adaptability for the future. Compared to existing liver phantoms, this work provides a more realistic region for needle insertion procedures due to the implementation of a ribcage. The results demonstrate the system's ability to simulate controlled motion and providing a realistic platform for testing and refining needle insertion procedures.

While the phantom achieves it's primary objectives, limitations such as actuator durability, lack of feedback control and general equipment malfunction were identified. These challenges can be enhanced and overcome in the future. In conclusion, this thesis represents a significant step forward in designing MRI-compatible anthropomorphic liver phantoms. While there are various improvements to be made, this work provides a solid foundation for future research and has the potential to improve various liver medical procedures.

Future work

Future work should focus on various key areas to make the system even more realistic and for general further enhancement. The pneumatic origami actuators were chosen for their ease of manufacturability. However, the current manufacturing method makes each actuator prone to leaks, which affect the performance of the motion. A different manufacturing method or a different design could be the solution to fixing a major issue of this setup.

By using digital regulators with greater pressure ranges, we can truly test the compression and extension capabilities of the actuators. Maybe a stiffer material of the actuator could also allow for more control with greater pressure ranges. At the same time, using a closed loop controller with real-time feedback could improve the precision of the liver movements and allow for more realistic representation of respiratory induced motion of the liver. The liver phantom could be "stopped" in various positions of SI and AP according to the needs of the medical practitioner. This would possibly allow for more realistic needle insertion procedure points (if the liver is further inside/outside of the ribcage perimeter). Using only one actuator in the SI direction would potentially allow for a greater range of motion, as using only one actuator would solve the flow issues that were encountered during this thesis.

A more realistic organ setup, with other gelatinous organs to support the liver from all around would be beneficial for physicians to train a variety of operations and procedures. Deformation could be integrated by testing "softer" materials for the liver and/or more boundaries in the setup that the liver can push up against. Future work could focus on overcoming these limitations and exploring additional applications for the phantom.

Finally, conducting tests with this setup in an MRI-environment in collaboration with clinicians would ensure the phantom's applicability in clinical scenarios. The system was tested with short pneumatic tubes of 1 m, but with longer tubes, the results of the motion will be different because of flow issues. More flow of air pressure is needed to sustain the motion. Longer tubes will be required to keep the Arduino and pressure regulators outside the MRI bore room, hence tests with representative pneumatic tube lengths need to be done.

Acknowledgements

First and foremost I would like to express my greatest thanks to Momen Abayazid for his invaluable guidance, expertise and support through this journey. His insights and advice have been instrumental in shaping this work.

I am equally thankful to Mostafa Selim, my first supervisor for his encouragement and for setting the foundation of the project with me, and to Ana Cordon, my second supervisor, for her continuous guidance and feedback throughout the entire thesis.

A special thanks goes to Rithwick Puranam, whom, although just started his PhD a few months ago, turned out to be one of the best daily supervisors anyone could ask for.

I am deeply appreciative of the technical support I received from Marjon Kuipers, Quentin Sablé and Artur Gąsienica whose expertise ensured that I could make the physical setup that sits in the lab today. Their contributions to this project have been invaluable.

Finally, I would like to sincerely thank all my family, friends, labmates, and housemates, whose unwavering support, encouragement, and camaraderie have been a source of strength throughout this journey. Your presence and understanding mean the world to me.

Thank you all for your invaluable contributions and support.

References

[1] S. Fahmi, F. F. Simonis, and M. Abayazid, "Respiratory motion estimation of the liver with abdominal motion as a surrogate", en, *The International Journal of Medical Robotics and Computer Assisted Surgery*, vol. 14, no. 6, L. Clive, Ed., e1940, Dec. 2018, ISSN: 14785951. DOI: 10.1002/rcs.1940. [Online]. Available: https://onlinelibrary.wiley.com/doi/10.1002/rcs.1940.

[2] C. DeMarco, *CT scan vs. MRI: What's the difference?*, en. [Online]. Available: https://www.mdanderson.org/cancerwise/ct-scan-vs-mri--what-is-the-difference.h00-159616278.html.

[3] *MRI Near Metal*, en-US, Jul. 2024. [Online]. Available: https://med.stanford.edu/bmrgroup/Research/mri-near-metal.html.

[4] M. S. Xavier, C. D. Tawk, A. Zolfagharian, *et al.*, "Soft Pneumatic Actuators: A Review of Design, Fabrication, Modeling, Sensing, Control and Applications", *IEEE Access*, vol. 10, pp. 59 442–59 485, 2022, ISSN: 2169-3536. DOI: 10.1109/ACCESS.2022.3179589. [Online]. Available: https://ieeexplore.ieee.org/document/9785890/.

[5] H. Naghibi, P. A. C. Costa, and M. Abayazid, "A Soft Robotic Phantom to Simulate the Dynamic Respiratory Motion of Human Liver", in *2018 7th IEEE International Conference on Biomedical Robotics and Biomechatronics (Biorob)*, Enschede: IEEE, Aug. 2018, pp. 577–582, ISBN: 978-1-5386-8183-1. DOI: 10.1109/BIOROB.2018.8488115. [Online]. Available: https://ieeexplore.ieee.org/document/8488115/.

[6] J. Yang, J. Cai, H. Wang, *et al.*, "Is Diaphragm Motion a Good Surrogate for Liver Tumor Motion?", en, *International Journal of Radiation Oncology*Biology*Physics*, vol. 90, no. 4, pp. 952–958, Nov. 2014, ISSN: 03603016. DOI: 10.1016/j.ijrobp.2014.07.028. [Online]. Available: https://linkinghub.elsevier.com/retrieve/pii/S0360301614035354.

[7] R. Song, A. Tipirneni, P. Johnson, R. B. Loeffler, and C. M. Hillenbrand, "Evaluation of respiratory liver and kidney movements for MRI navigator gating", en, *Journal of Magnetic Resonance Imaging*, vol. 33, no. 1, pp. 143–148, Jan. 2011, ISSN: 1053-1807, 1522-2586. DOI: 10.1002/jmri.22418. [Online]. Available: https://onlinelibrary.wiley.com/doi/10.1002/jmri.22418 (visited on 12/02/2024).

[8] A. Cordón Avila and M. Abayazid, "Liver respiratory-induced motion estimation using abdominal surface displacement as a surrogate: Robotic phantom and clinical validation with varied correspondence models", en, *International Journal of Computer Assisted Radiology and Surgery*, vol. 19, no. 8, pp. 1477–1487, May 2024, ISSN: 1861-6429. DOI: 10.1007/s11548-024-03176-1. [Online]. Available: https://link.springer.com/10.1007/s11548-024-03176-1.

[9] J. L. Hinshaw, A. M. Shadid, S. Y. Nakada, S. P. Hedican, T. C. Winter, and F. T. Lee, "Comparison of Percutaneous and Laparoscopic Cryoablation for the Treatment of Solid Renal Masses", *American Journal of Roentgenology*, vol. 191, no. 4, pp. 1159–1168, Oct. 2008, Publisher: American Roentgen Ray Society, ISSN: 0361-803X. DOI: 10.2214/AJR.07.3706. [Online]. Available: https://ajronline.org/doi/10.2214/AJR.07.3706.

[10] Y. X. Mak, A. Dijkshoorn, and M. Abayazid, "Design Methodology for a 3D Printable Multi-Degree of Freedom Soft Actuator Using Geometric Origami Patterns", en, *Advanced Intelligent Systems*, vol. 6, no. 6, p. 2 300 666, Jun. 2024, ISSN: 2640-4567, 2640-4567. DOI: 10.1002/aisy.202300666. [Online]. Available: https://onlinelibrary.wiley.com/doi/10.1002/aisy.202300666.

[11] R. Obbink, "Learning feed-forward control for a Soft Robotics phantom to simulate respiratory liver motion.pdf", English, University of Twente, Enschede, Individual Assignment Report 016RAM2019, May 2019, Committee: Dr.ir. H. Naghibi Beidokhti, Dr.ir. M. Abayazid.

[12] T. L. De Jong, A. Moelker, J. Dankelman, and J. J. Van Den Dobbelsteen, "Designing and validating a PVA liver phantom with respiratory motion for needle-based interventions", en, *International Journal of Computer Assisted Radiology and Surgery*, vol. 14, no. 12, pp. 2177–2186, Dec. 2019, ISSN: 1861-6410, 1861-6429. DOI: 10.1007/s11548-019-02029-6. [Online]. Available: http://link.springer.com/10.1007/s11548-019-02029-6.

[13] T. L. De Jong, L. H. Pluymen, D. J. Van Gerwen, G.-J. Kleinrensink, J. Dankelman, and J. J. Van Den Dobbelsteen, "PVA matches human liver in needle-tissue interaction", en, *Journal of the Mechanical Behavior of Biomedical Materials*, vol. 69, pp. 223–228, May 2017, ISSN: 17516161. DOI: 10.1016/j.jmbbm.2017.01.014. [Online]. Available: https://linkinghub.elsevier.com/retrieve/pii/S1751616117300218 (visited on 12/07/2024).

[14] D. C. Wolf, "Evaluation of the Size, Shape, and Consistency of the Liver", eng, in *Clinical Methods: The History, Physical, and Laboratory Examinations*, H. K. Walker, W. D. Hall, and J. W. Hurst, Eds., 3rd, Boston: Butterworths, 1990, ISBN: 978-0-409-90077-4. [Online]. Available: http://www.ncbi.nlm.nih.gov/books/NBK421/.

[15] T. Kato, K. Takemasa, T. Ikeda, *et al.*, "Analysis of respiratory-induced motion trajectories of individual liver segments in patients with hepatocellular carcinoma", en, *Journal of Applied Clinical Medical Physics*, vol. 25, no. 4, e14257, Apr. 2024, ISSN: 1526-9914, 1526-9914. DOI: 10.1002/acm2.14257. [Online]. Available: https://aapm.onlinelibrary.wiley.com/doi/10.1002/acm2.14257.

[16] A. U. INC, "TPU-92A Technical Data Sheet", Kimya, a division of ARMOR Group, Tech. Rep., Jul. 2019. [Online]. Available: https://www.kimya.fr/wp-content/uploads/2019/10/kimya_fiche_TPU-92A-US-EN.pdf.

[17] F. Inc, "Elastic 50A Technical Data Sheet", Tech. Rep., Oct. 2020. [Online]. Available: https://formlabs-media.formlabs.com/datasheets/2001420-TDS-ENUS-0.pdf.

[18] *Tracker Video Analysis and Modeling Tool for Physics Education*. [Online]. Available: https://physlets.org/tracker/.

[19] *Automatiseringstechnologie en technische onderwijsoplossingen | Festo NL*. [Online]. Available: https://www.festo.com/nl/nl/.

A General Appendix

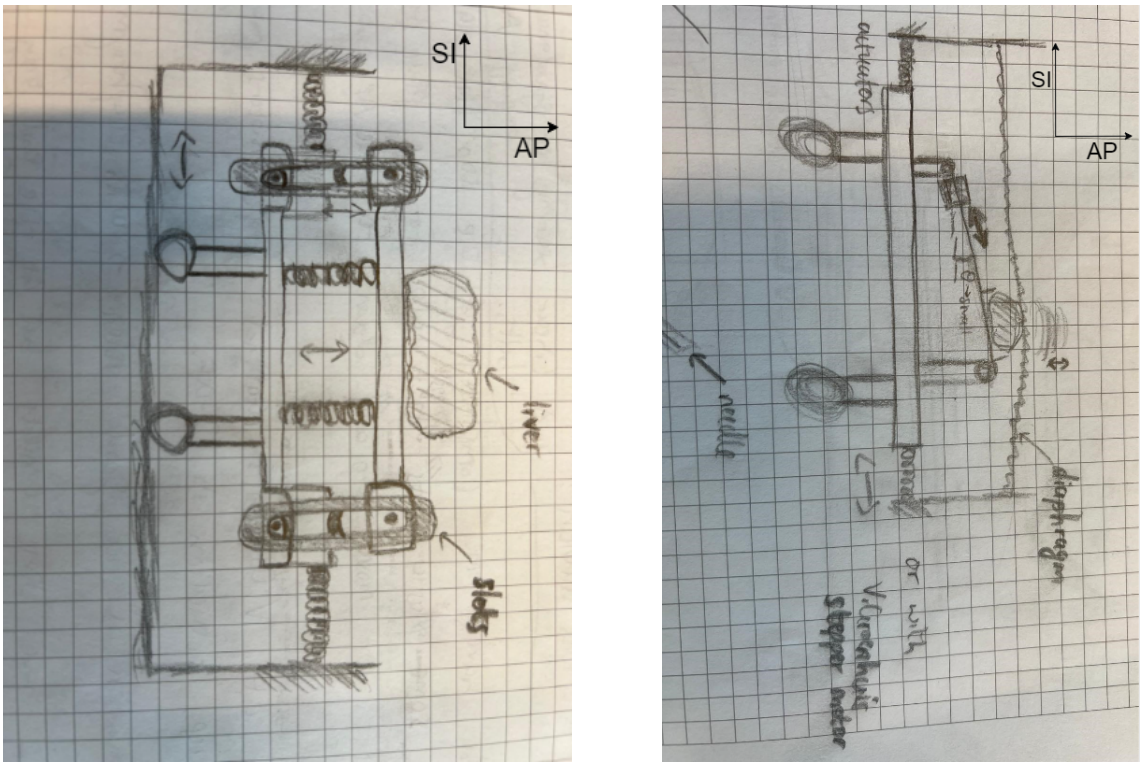

(a) First concept sketch

(b) Second concept sketch

Figure 21: Initial sketches for concepts

The first concept sketch shows a different mechanism to the scissor linkages of the previous liver phantom shown in Figure 2. In this concept, laser cut slots with stop limits would be use to control the actuation of the SI direction. This concept was not chosen due to the SI direction slots not being rigid enough. There would have been extra compliancy in the SI direction, leading to the top plate, shifting position either to the left or right with reference to the bottom plate.

The second concept was one which required only actuators in the SI direction and use of a pulley system for the AP direction, rather than pneumatic actuation. This concept also involved the use of a diaphragm (rather, a skin layer) that would act as a boundary against which the liver would deform. This concept was not chosen, due to the high complexity of integrating a pulley system that would be able to hoist a human-sized liver within the given spatial requirements of the respiratory motion phantom. In addition, the skin layer would not provide an accurate deformation of the liver and was therefore considered redundant.

Figure 23: Actuator with elastic resin coating

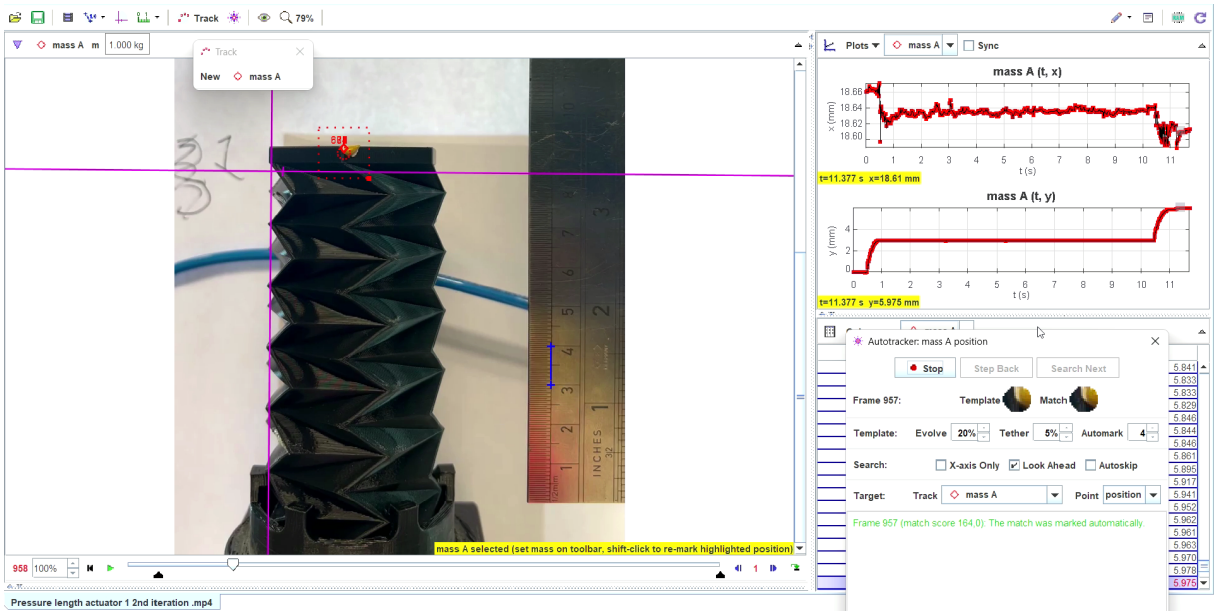

Figure 24: Analysis of a pressure-length video in Tracker. The motion can be seen on the right side in the y-axis. This movement data is then exported as a .csv file into MATLAB and then analysed to produce the graphs seen in section 5

B Solidworks files

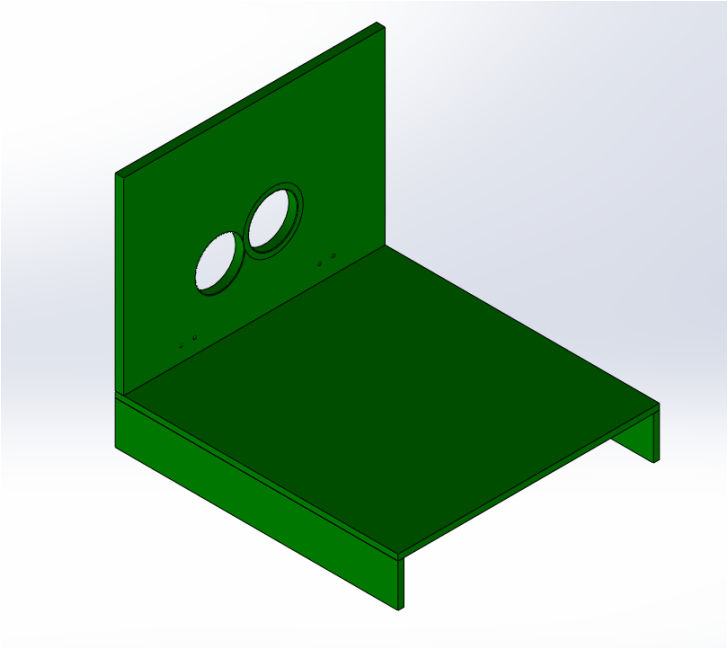

Figure 25: Base of phantom setup

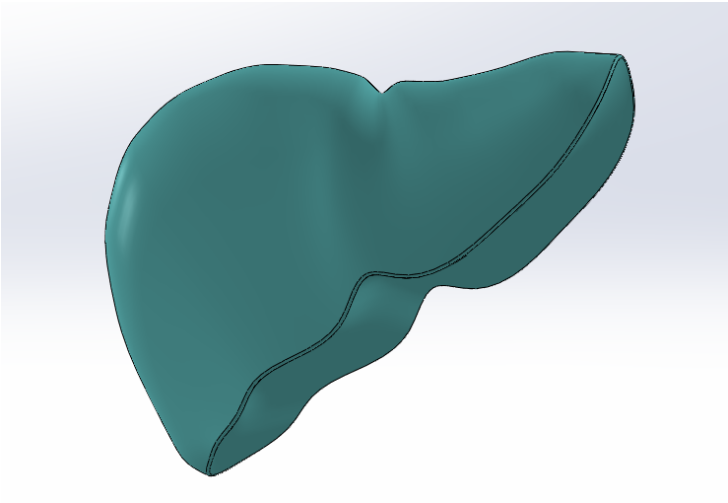

Figure 26: Liver phantom model

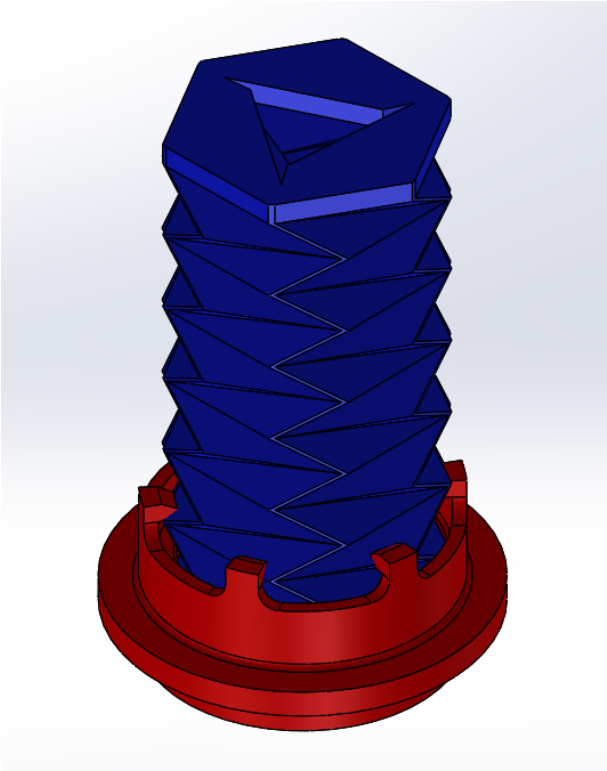

Figure 27: Actuator sitting in actuator clamp

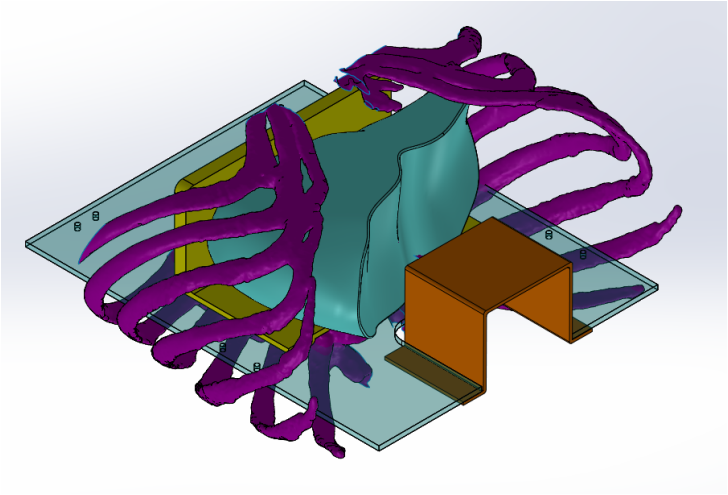

Figure 28: Inner rib plate (transparent cyan) with diaphragm plate (yellow), liver (cyan) and AP actuator shelf (orange) surrounded by ribcage (purple)

C Experiment Results

Shown below is the raw data that was used to create the final graphs seen in Figure 13 and Figure 16. The following are graphs of the raw data points for each actuator, with the respective experiment done 3 times for each.

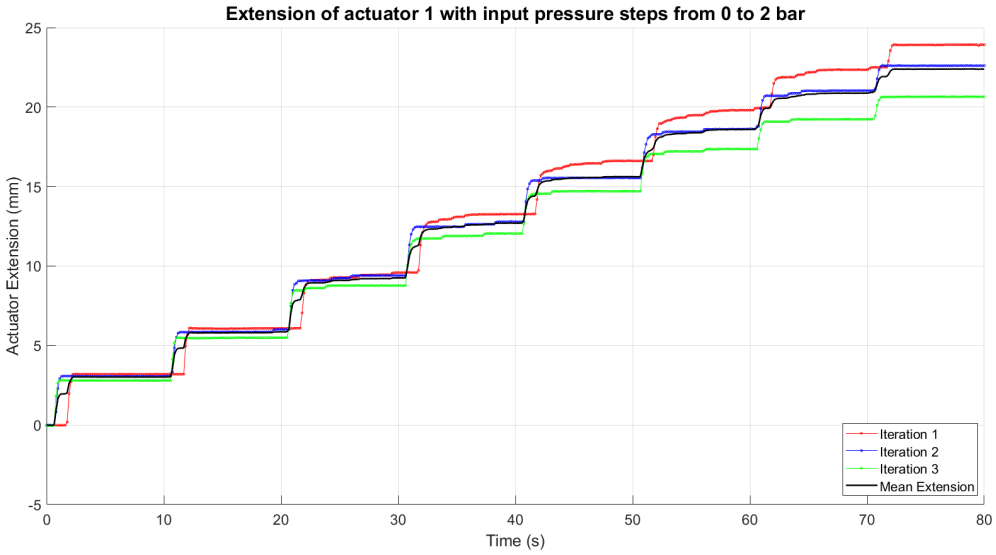

Figure 29: Pressure-length values actuator 1

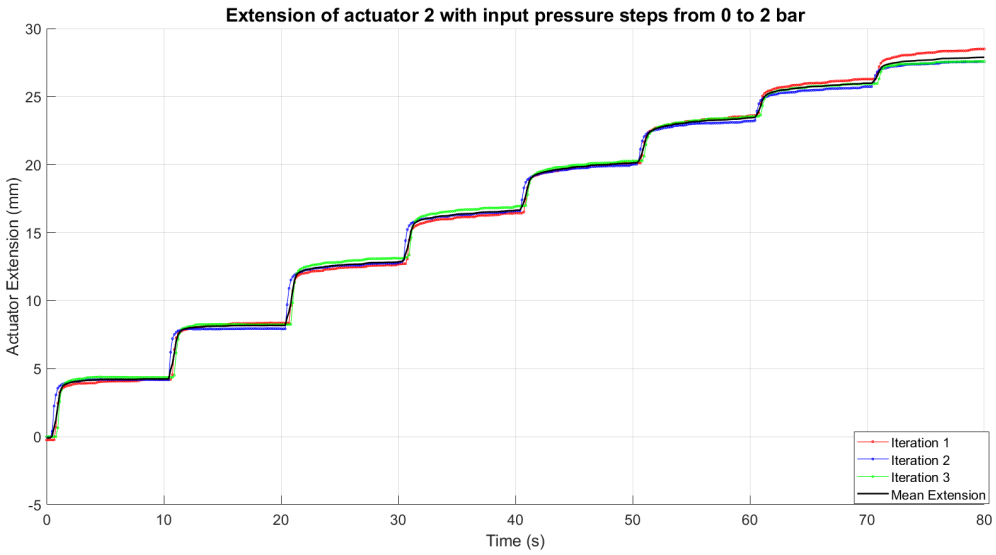

Figure 30: Pressure-length values actuator 2

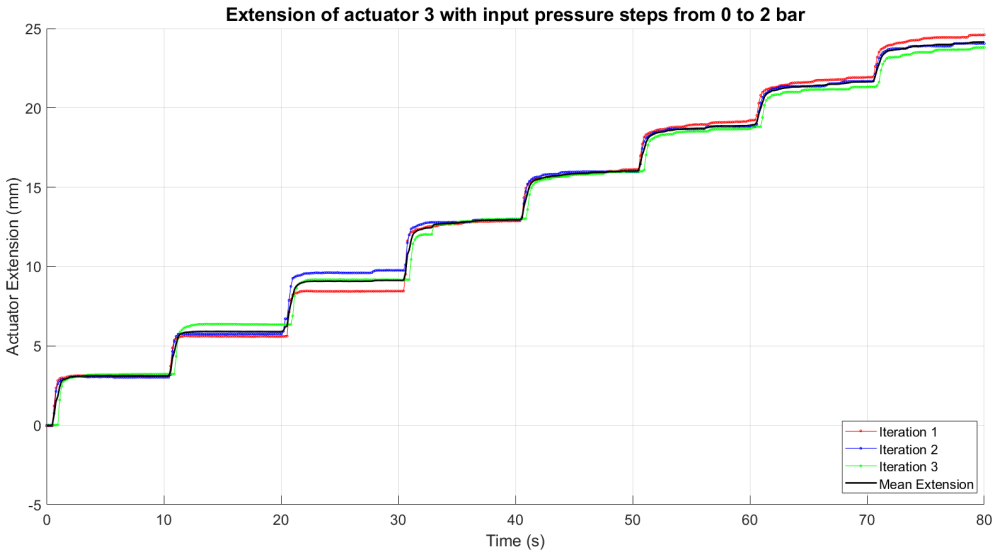

Figure 31: Pressure-length values actuator 3

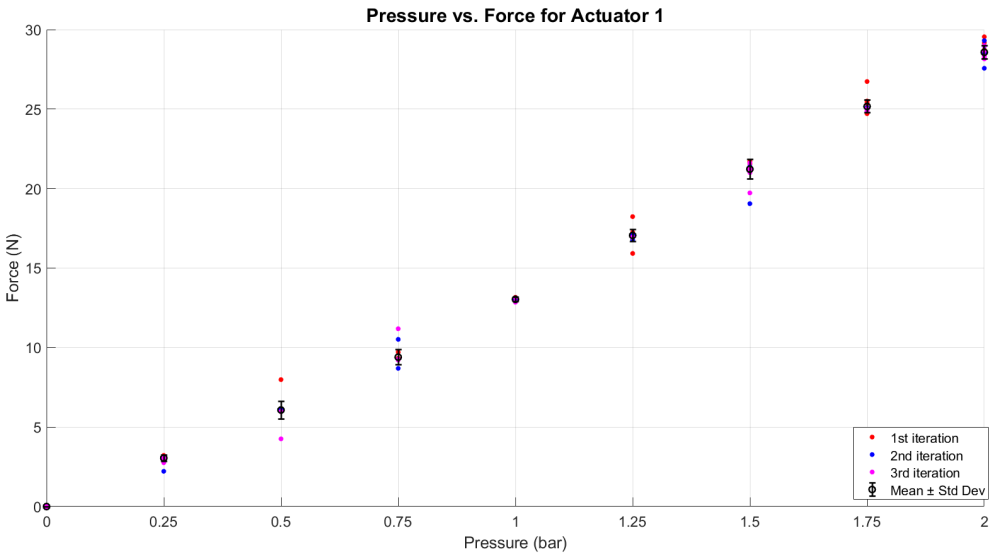

Figure 32: Pressure-force values actuator 1

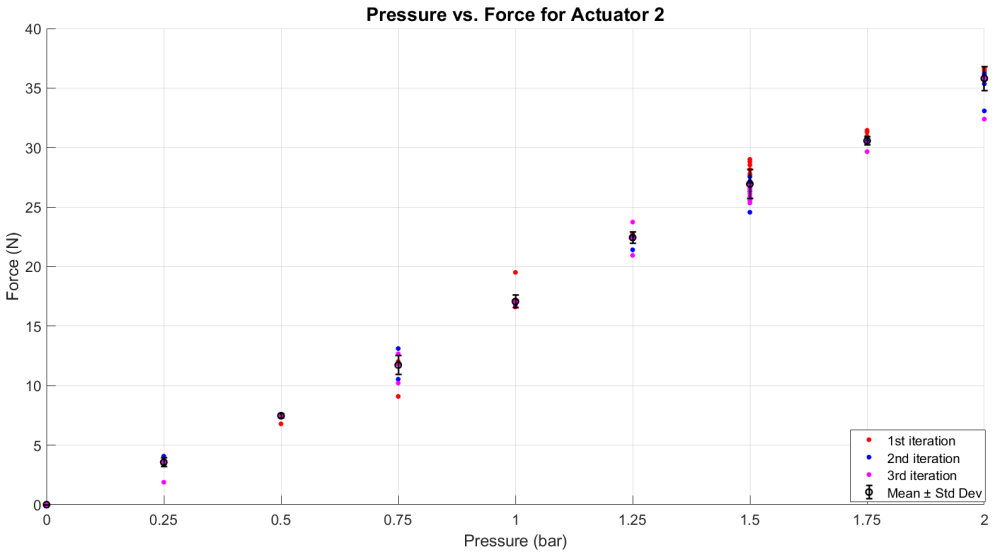

Figure 33: Pressure-force values actuator 2

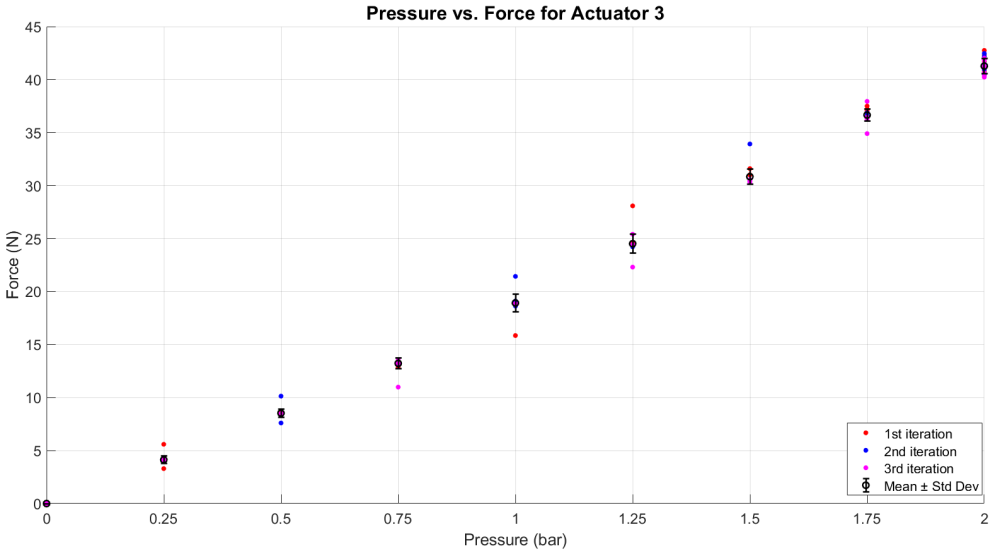

Figure 34: Pressure-force values actuator 3

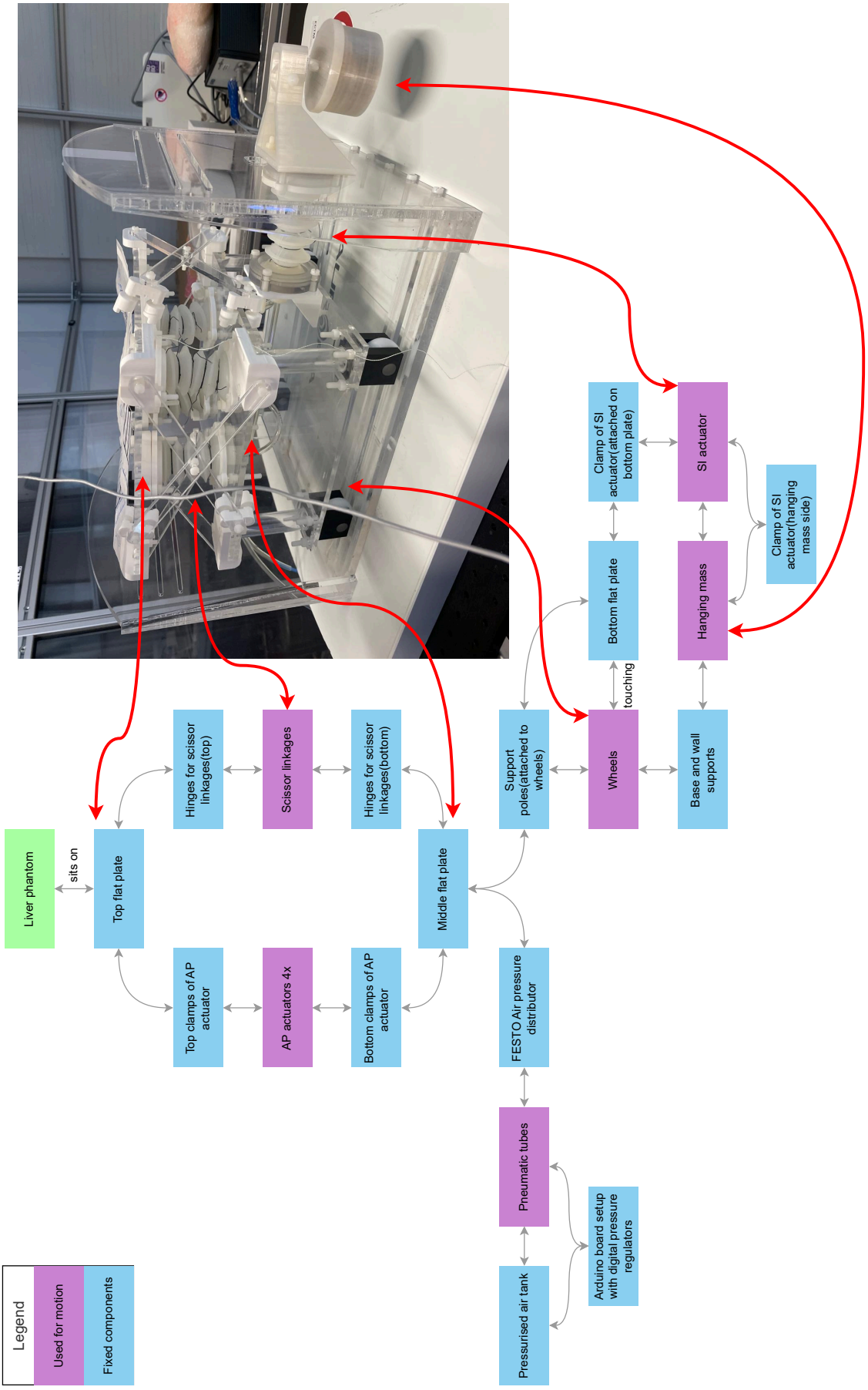

Figure 22: Component and interaction diagram of old phantom setup